Faculty of Electrical Engineering
Department of Electric Drives and Traction

Bachelor's thesis

Electropermanent Magnet Study

Veronika Mártonová

January 2019

Supervisor: Ing. Pavel Kobrle, Ph.D.

ZADÁNÍ BAKALÁŘSKÉ PRÁCE

I. OSOBNÍ A STUDIJNÍ ÚDAJE

Příjmení: **Mártonová** Jméno: **Veronika** Osobní číslo: **380820**

Fakulta/ústav: **Fakulta elektrotechnická**

Zadávající katedra/ústav: **Katedra elektrických pohonů a trakce**

Studijní program: **Elektrotechnika, energetika a management**

Studijní obor: **Aplikovaná elektrotechnika**

II. ÚDAJE K BAKALÁŘSKÉ PRÁCI

Název bakalářské práce:

Studium elektropermanentního magnetu

Název bakalářské práce anglicky:

Electropermanent Magnet Study

Pokyny pro vypracování:

1. Seznamte se s principem funkce elektropermanentního magnetu a stručně jej popište.
2. Zaměřte se též na možné využití elektropermanentních magnetů v praxi.
3. Prostudujte problematiku návrhu elektropermanentního magnetu.
4. Vytvořte vhodný simulační model, kterým demonstrujete funkci elektropermanentního magnetu.

Seznam doporučené literatury:

[1] Knaian, A. N.: Electropermanent Magnetic Connectors and Actuators: Devices and Their Application in Programmable Matter. Dissertation thesis. Massachusetts Institute of Technology, 2010.
[2] Fitzgerald, A. E., Kingsley, C. and Umans, S. D.: Electric Machinery, McGraw-Hill, New York, NY, 2002.
[3] Marchese, A. D., Asada, H. and Rus, D.: Controlling the locomotion of a separated inner robot from an outer robot using electropermanent magnets. IEEE International Conference on Robotics and Automation (ICRA), 2012, pp. 3763-3770.

Jméno a pracoviště vedoucí(ho) bakalářské práce:

Ing. Pavel Kobrle, Ph.D., katedra elektrických pohonů a trakce

Jméno a pracoviště druhé(ho) vedoucí(ho) nebo konzultanta(ky) bakalářské práce:

Datum zadání bakalářské práce: **07.09.2018** Termín odevzdání bakalářské práce: _____

Platnost zadání bakalářské práce: **30.09.2019**

Ing. Pavel Kobrle, Ph.D. podpis vedoucí(ho) práce	podpis vedoucí(ho) ústavu/katedry	prof. Ing. Pavel Ripka, CSc. podpis děkana(ky)

III. PŘEVZETÍ ZADÁNÍ

Studentka bere na vědomí, že je povinna vypracovat bakalářskou práci samostatně, bez cizí pomoci, s výjimkou poskytnutých konzultací. Seznam použité literatury, jiných pramenů a jmen konzultantů je třeba uvést v bakalářské práci.

. _____
Datum převzetí zadání

_____
Podpis studentky

Declaration

I declare that the presented work was developed independently and that I have listed all sources of the information used within it in accordance with the methodical instructions for observing the ethical principles in the preparation of university theses.

Prague, January 3, 2019

. . . . . .
Veronika Mártonová

Acknowledgement

I would like to express thanks to my thesis supervisor, Pavel Kobrle. He taught me a lot, e.g., how not to take the difficulties of life so seriously, and supported me in every aspect of my studies. I would like to express thanks to Petr Čížek. He encouraged me, supported me and shared the joys and the worries during my studies. Last but not least, I would like to thank my family for a full support throughout my studies at the Czech Technical University. And thank to God that I have finally finished it.

Abstrakt

Bakalářská práce pojednává o problematice elektropermanentního magnetu (EPM). Obsahuje teoretickou, výpočetní i experimentální část. Kapitoly teoretické části vysvětlují princip EPM, popisují jeho výhody a nevýhody, a věnují se možným použitím EPM v praxi. Odvození matematicko-fyzikálních vztahů pro návrh EPM, návrh konkrétního zařízení s funkcí EPM a simulace ověřující teoretické principy jeho provozních stavů jsou obsaženy ve výpočetní části. Pro simulaci bylo zvoleno prostředí ANSYS Maxwell. V experimentální části jsou pak uvedeny a diskutovány výsledky měření, které dokládají správnost návrhu, spolu s porovnáním mezi teoretickým výpočtem, simulací a praktickým experimentem.

Klíčová slova: magnetismus, permanentní magnet, elektromagnet, elektropermanentní magnet (EPM), princip EPM, ANSYS Maxwell

Abstract

This thesis focuses on the principle of operation, description and experimental verification of the electropermanent magnet (EPM), which is a solid-state device whose external magnetic flux can be stably switched on and off by a discrete electrical pulse. The thesis is divided into the theoretical, computational and experimental parts. The theoretical part describes the EPM principle of operation and lists its advantages, disadvantages and application potentials. Next, a mathematical-physical model of the EPM device is derived in the computational part. The computational part also contains the specifications for the design of a real EPM device and simulations, carried out in the realistic simulator ANSYS Maxwell, that verify the EPM functionality and support the derived theoretical relations. Finally, the experimental part reports on the experimental evaluation with a real EPM device, made according to the presented specifications, together with the description and comparison to the theoretical and simulated results.

Keywords: magnetism, permanent magnet, electromagnet, electropermanent magnet (EPM), EPM principle, ANSYS Maxwell

Contents

List of Figures

List of Tables

Chapter 1
Introduction

This thesis focuses on the study of the electropermanent magnets. Electropermanent magnet is an interesting combination of the electromagnet and permanent magnet. The principle of the electropermanent magnet is that it can alternate its external magnetic flux between the "ON" state and "OFF" state due to a discrete electrical pulse. The main advantage of the electropermanent magnet is that the energy is consumed only during the switching between the states.

The thesis is divided into four main chapters. The first Chapter is dedicated to the general introduction and the history of the magnetism. Chapter 2 describes the principle of the electropermanent magnet operation. It also lists the advantages and disadvantages, as well as, the practical use of the electropermanent magnets. Moreover, the use cases of the electropermanent magnet that are under development are mentioned. Chapter 3 focuses on the expression of the mathematical-physical relations and the main parameters for designing of the electropermanent magnet device. A part of this chapter is dedicated to the description of the material properties of used materials for the designed device. Chapter 4 deals with the simulation of the electropermanent magnet device in the realistic simulator ANSYS Maxwell, and it also presents the experimental evaluation of the designed prototype of the electropermanent magnet. The experimental evaluation is followed by a thorough discussion and comparison to the theoretical and simulated results. The thesis is concluded by the last part which summarizes the results and provides remarks for future improvements and development of the electropermanent magnets.

1.1 Motivation and Goals

The motivation behind the thesis is to create a new type of robotic actuators or artificial muscle tendons. Under such a perspective, the electropermanent magnets appear to be an interesting and underestimated technology. For the field of robotics, it is necessary to find novel actuators which can provide minimal consumption of energy in the state when the robots do not need to move. An example of the typical robotic actuator can be the servo motors. When a quadruped robot is only staying at a place and does not move, all its servo motors consume the energy just for holding of the legs in given positions. Therefore, it is reasonable to seek for the novel actuators which do not consume energy at such situations. This is just a single example out of many to be found in the engineering practice. Some of them are further described in the thesis, but others still wait for discovering.

The electropermanent magnets, as will be explained later, alternate between the two basic states, in which they do not need the power supply. Therefore, they were chosen for the exploration in this field.

The goal of this thesis is not to develop an actual actuator, but to become familiar with this technology and to find the advantages and disadvantages of their usage. The main goal is to explain the principle of operation of the electropermanent magnets, to find applications, where the technology could be used in everyday life. The second goal is to derive specifications for the design of an electropermanent magnet device and try to manufacture a prototype to find out its pitfalls. The third goal is to use an appropriate model to simulate the electropermanent magnet to demonstrate and verify its functions. Beyond the set objectives, the experimental evaluation of a real prototype of the electropermanent magnet function is done.

1.2 Magnetism and Magnets

Magnetism is the physical phenomena mediated by a magnetic field. All materials exhibit magnetic properties to some extent. However, this phenomenon is most easily observable on the material group called ferromagnetic materials, e.g. iron, nickel, and cobalt.

Historically, magnetism has been observed spontaneously when people noticed that lodestones, naturally magnetized pieces of the mineral magnetite, attract iron. Later on, this phenomenon was clarified to be a natural material property caused by the spin magnetic moments of elementary particles. The discovery of the relationship between magnetism and electricity was a significant breakthrough in the study of magnetism. The relationship was discovered by Hans Christian Ørsted at the beginning of the 19^{th} century [1]. He observed the accidental twitching of a compass needle near the wire passed by an electric current. Later on, he proved that the magnetic field is produced by an electric current flowing through the coil.

The discovery of the principle inspired many other scientists, such as Ampere, Faraday, and Maxwell, and started a new epoch of technological progress. Every day, we encounter devices that work on this principle, such as motors, transformers, magnetic levitation as well as magnetic recording and data storage equipment, etc.

Depending on the source of magnetism, magnets can be divided into two main groups - permanent magnets and electromagnets. Permanent magnets do not need external influences to create a persistent magnetic field. Some rocks, as lodestone (see Figure 1a), exhibit magnetic properties naturally, but magnets can also be made industrially [2].

The artificial permanent magnets are typically made from iron or nickel alloys (see Figure 1b). They are made by inserting the material into an external magnetic field which forces the magnetic domains in the material to orient identically. As a result, the material starts to exhibit magnetic properties and retain them until the critical temperature is reached, called the Curie temperature (e.g. 770 °C for iron). The material loses its magnetic effects when this temperature is exceeded [3].

The second group of magnets is the electromagnets. The electromagnet consists of a coil with a core made from "soft" magnetic material, used to create a temporary magnetic field. When the current flows through the coil, the core is magnetized and starts to behave like a magnet - the core has the northern and the southern pole. If the current stops flowing through the coil, the core loses its magnetic effects either immediately, or it may remain partially magnetized and loses the rest of its magnetization with the time [4]. Figure 1c shows a basic example of an electromagnet made from a common nail, copper coil, and a battery power source.

The electropermanent magnets (EPM) are the specific type of permanent magnets with a non-traditional construction that allows them to exhibit properties that closely resemble the behavior of electromagnets. This thesis deals with this type of magnets and following chapters are devoted to their functional description, modeling, simulation, and construction.

(a) The lodestone. Courtessy of [5].

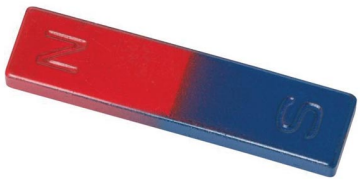

(b) The artificial magnet made from iron. Courtessy of [6].

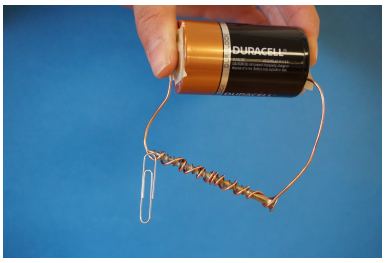

(c) The basic electromagnet. Courtessy of [7].

Figure 1: Examples of the magnets.

Chapter 2
Electropermanent Magnet

The principle of the electropermanent magnet operation is explained in this chapter together with its advantages and disadvantages and comparisons to similar technologies. Further, application potentials and use cases are described.

The electropermanent magnet (EPM) is a type of permanent magnet with a special behavior of the external magnetic field. In particular, the EPM can be used in two states - when the external magnetic field is on or off.

Scheme of the EPM is visualized in Figure 2. The EPM consists of two separate magnets connected by two plates. Plates have permeability higher than that of air and they are usually made from iron alloy. The magnets have the following properties. The first property is that both of the magnets have approximately the same residual magnetization. The second property is that the magnets have different coercivity. These properties are fulfilled in the case the first magnet is “hard” and the second one is “soft”. The operation of the EPM is based on these properties, which are described in Section 2.1, and the principle of operation is further detailed in Section 2.2. The coil wrapped around the “soft” magnet serves the purpose of switching between the states when the external magnetic field of the EPM is switched on and off.

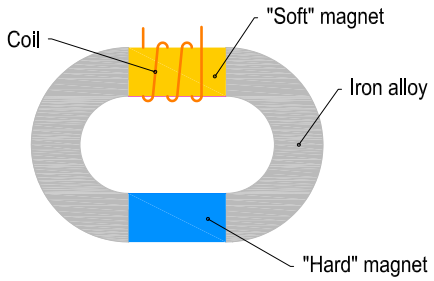

Figure 2: Electropermanent magnet.

2.1 Magnetic Hysteresis Loop

To grasp the principle of the EPM, we need to understand the basic electromagnetic properties of the magnetic flux density B and the magnetic field intensity H that are related by the so-called magnetic hysteresis loop or “B-H curve”. The “B-H curve” is different for every material [8] and has six important points given by the magnetization cycle of the material. The magnetization cycle of a ferromagnetic material is visualized in Figure 3 and it behaves as follows [9].

We obtain the first point by inserting ferromagnetic material, that has not been previously magnetized ($B = 0, H = 0$), into the magnetic field induced by a coil passed by electric current. When the magnetization current in the coil is increased in the positive direction, the material is magnetized according to the initial magnetization curve up to the point of full saturation (point **a**).

Afterward, the magnetization current in the coil is reduced to zero which implies that the magnetic field intensity is also reduced to zero. But the magnetic flux in the ferromagnetic material will not reach zero due to the residual magnetism in the material as it is shown on the curve from the point

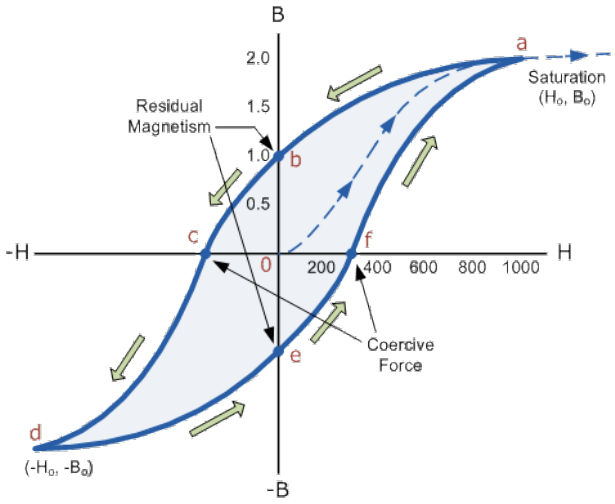

Figure 3: Magnetic hysteresis loop. Courtesy of [10].

a to the point **b**. The magnetic flux density at the point **b** has the value B_r and it is called remanent magnetism. Remanent magnetism in the "soft" magnetic materials decreases over a longer period due to the temperature while the "hard" magnetic materials maintain the residual magnetism.

If we start to demagnetize the material until the material ceases to exhibit magnetic effects, we get the point **c**. It means the magnetization current in the coil is increased in the negative direction. The magnetic flux density B equals zero and the intensity of the magnetic field is equal to coercive force H_C (a.k.a. coercivity). The coercive force is the measure of the ability of the material to withstand the external magnetic field without getting demagnetized. The next point **d** of the full saturation in the opposite direction is reached by a further increase of the current in the coil. Now, we can close the curve by the same procedure as described above.

When turning off the source of the magnetization current in the coil, we get the point **e**. By the further increase of the magnetization current in the opposite direction we get the point **f** and then the point **a** again.

We can recognize the "hard" or "soft" magnetic material based on the width of the magnetic hysteresis loop. The narrow magnetic hysteresis loop is typical for the "soft" magnetic materials whereas the wide "B-H curve" is typical for the "hard" magnetic materials (see Figure 4).

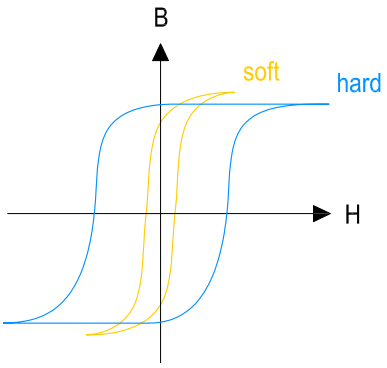

Figure 4: Typical shape of the "B-H curve" for "soft" and "hard" magnetic materials.

2.2 Principle of Electropermanent Magnet

The principle of operation of the EPM can be shown on an example visualized in Figure 5. The figure shows two common magnets connected by the horseshoe plates made from an iron alloy. When the two magnets are arranged such as their orientation is opposite, the field lines are going from the southern pole of the first magnet through the iron plate to the northern pole of the second magnet and further from the southern pole of the second magnet through the second iron plate to the northern pole of the first magnet as can be seen in Figure 5a. This state is denoted as the "OFF" configuration as the field lines close through the body of the EPM. On the other hand, when the second magnet changes its orientation, thus both the magnets are arranged in an agreeing configuration, the horseshoe plates act as poles of a single magnet, and the field lines start to close outside of the device body, as it is visualized in Figure 5b. This state is denoted as the "ON" configuration.

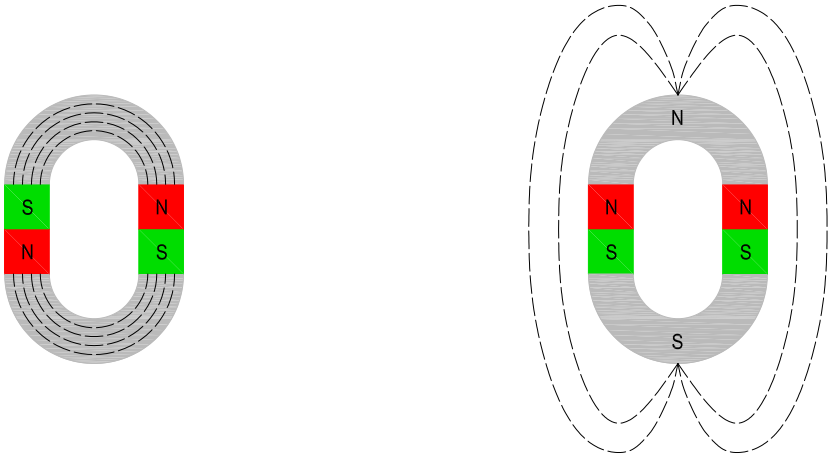

(a) "OFF" state. (b) "ON" state.

Figure 5: Two basic states of the electropermanent magnet. Both of the magnets are from the "hard" magnetic material and the southern pole is marked as "S" in the green area. The northern pole is marked as "N" in the red area. The grey horseshoe represents the iron alloy.

While it is possible to alternate the orientation of the second magnet mechanically by rotating it, it is also possible to exploit different material properties of the magnetic-soft and magnetic-hard materials. In particular, the ferromagnetic materials with the narrow magnetic hysteresis loop have the value of the coercive force much lower than the materials with the wide hysteresis loop as described in Section 2.1. Hence, by substituting one of the magnets in the structure depicted in Figure 5 by "hard" magnetic material and the second one by "soft" magnetic material wrapped by the coil it is possible to use the remagnetization of the soft magnet by a magnetization current pulse in the coil which will alternate the polarity of that magnet.

Figure 6a depicts the EPM device in "OFF" state, where the "soft" and the "hard" magnets have opposite magnetization which makes the magnetic field lines close inside the body of the EPM formed by the two magnets and plates. We reach the "ON" configuration by remagnetization of the "soft" magnet using the following procedure. The magnetization current increases in the coil in the positive direction for a short period, which is called the switching current pulse. The pulse length depends on the value of the coercive force. The polarity of the "soft" magnet is changed over the duration of the switching current pulse while the polarity of the "hard" magnet remains the same. The magnets assembly get the character of a single large magnet and the iron plates become new poles as in the previous example. The magnetic flux will start to close through the air outside of the EPM body, thus we gain the external magnetic field as it is visualized in Figure 6b. We use the switching current pulse in the coil in the negative direction for re-achievement of the "OFF" configuration.

Thanks to this principle, we can alternate the “ON” state and “OFF” state as often as we want. The speed of alternation between the states is limited only by the speed of polarity change of the “soft” magnet.

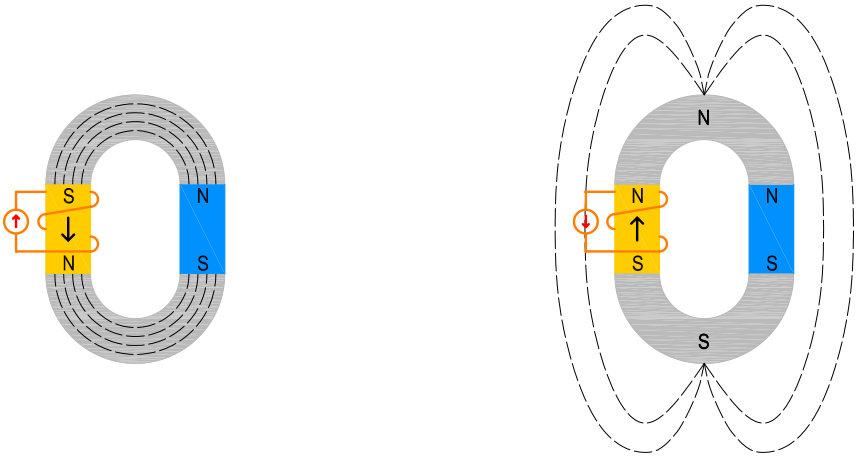

(a) “OFF” state. (b) “ON” state.

Figure 6: The “ON” and the “OFF” states of the EPM switched by switching current pulse. The yellow rectangle represents the “soft” magnet and the “hard” magnet is represented by the blue rectangle. The northern pole is marked as “N” and the southern pole is denoted as “S”. The red arrow shows the direction of the switching current and the black arrow represents the direction of the magnetic flux.

It is important to mention some differences of electropermanent magnets in technical practice. The magnets are usually not connected by the horseshoe plates, as the plates have different shapes based on the particular purpose of the EPM. Another difference is the location of the coil, as both magnets can be wrapped in the same coil because the EPMs are often used in small form factors and therefore it is easier to wrap the coil around both magnets. Therefore, the magnets must have different coercivity because during the change of the polarity of the first magnet the polarity of the second one has to remain the same. Therefore, the EPMs are built using the combination of “hard” and “soft” magnets.

Further, it is beneficial to use the magnets with similar residual magnetization for reducing the leakage magnetic flux which may cause an unwanted adhesion to another material in the “OFF” state. Therefore, we are looking for the combination of the “hard” magnet and the “soft” magnet for the EPM that have almost the same residual magnetization while having different coercive force. Based on these constraints, the Aluminum-Nickel-Cobalt alloy and the Neodymium-Iron-Boron alloy are typically used for the “soft” magnets and the “hard” magnets respectively. These two materials satisfy the requirements above and will be further described in Section 3.2.

2.3 Use of Electropermanent Magnets

Generally, magnets are used for connecting two, or more, materials. Hence, it is possible to call these magnets the joining devices. This section intends to answer the question of why to use the electropermanent magnets for this type of connections. Furthermore, the advantages and disadvantages of the EPM together with the application potentials and use cases are described in this section.

2.3.1 Joining Options

Generally, there are three existing approaches on how to connect the materials - chemical, mechanical and physical [11]. The additional methods are the combination of the basic principles listed above. Chemical forces originate from chemical reactions between the materials. Mechanical forces arise

from interlocking and resulting interference between parts without any need for chemical or physical (or electromagnetic) interaction and finally, the naturally occurring attraction between atoms, oppositely charged ions, and molecules leads to bond formation and joining due to physical forces [11]. Example of the chemical forces is adhesive bonding, mechanical forces arise, e.g. between the mechanical joints, and an example of physical connection is welding.

There are many ways to approach the problem of materials joining. The specific method for joining two materials depends on lots of material and environmental properties, e.g. the material types, the ambient temperature, the humidity, etc. Another important decision is whether we want to create a permanent or a temporary connection. In most cases, we can consider the chemical and physical connection as a permanent. Stability of the mechanical connection depends on the particular system of joining. But electromagnetic connections are the special type of physical connections and it is possible to consider them temporary.

It is impossible to divide and evaluate all types of connections. Therefore, we will focus on the evaluation of connection types which are only temporary. This condition is particularly suitable for the following connections:

- mechanical joints,
- electrostatic connections,
- magnetic and electromagnetic connections.

Mechanical joints have the advantage that they can have more degrees of freedom and thus make it easier to manipulate them. Another advantage is their ability to transfer large forces. On the other hand, the disadvantage is difficult fabrication due to their complexity. Next, the joints easily wear out and the binding can become loose over time. Besides, the connection can be difficult to break in case of complicated joints. Electrostatics also come into consideration, but its disadvantage is that it produces very little strength.

The permanent magnets, electropermanent magnets, and electromagnets create the electromagnetic connections. The main advantages of these types of devices are that the connection can be made temporary and can be easily controlled. The effect of electromagnetic connection may be canceled by demagnetization or by a mechanical device. Low-cost, high holding force in relation to the magnet dimensions and durability are the main benefits of magnetic devices. Next section focuses on the comparison of EPM with permanent magnets and electromagnets and shows its advantages and disadvantages.

2.3.2 Advantages and Disadvantages of Using Electropermanent Magnet

Magnets are used mostly as gripper devices, as mentioned above. One of the most exciting properties of the EPM is its scalability. The energy required to switch the state of an EPM is proportional to its volume, while the force it can excerpt scales with its area.

The next advantage of using EPM is the creation of temporary connection between two ferromagnetic materials that can be easily controlled in comparison to the permanent magnets that can create a temporary connection as well, but a dedicated mechanical device is necessary to cancel the connection by, e.g. a special screw which ensures a sufficient spacing between the permanent magnet and the drawn material. In the case of a really strong magnet, this option is unnecessarily complicated.

The other option is using electromagnets. In such a case, the connection canceling is easy - it requires only disconnecting the power supply of the coil. On the other hand, we spend money on the holding force for the whole duration of the connection. Therefore, the EPM is a convenient combination of the advantages of both of the previous methods. We use permanent magnet properties during the duration of the connection and when we need to interrupt the connection, we use the electrical energy to change the state from the “ON” state to the “OFF” state by the switching current. Unlike

electromagnets, the current flowing through the coil is truncated to a pulse that lasts only for a few milliseconds (for further details see Section 3.5).

Moreover, EPMs and electromagnets allow for control of the holding force unlike the permanent magnets [12]. Another advantage is that the EPM does not heat up due to a short switching pulse in comparison to electromagnets which heat up due to the magnetizing current flowing through the coil.

The main disadvantage of the EPM is a small radius of the produced external magnetic field. The force decreases exponentially with the increasing size of the air gap between the EPM and the target surface [13, 14]. This is shown in Figure 7. However, this can also be viewed as a feature in comparison to other connectivity options (e.g. chemical or mechanical) while this property allows to retaining other materials even at greater distances (e.g. the principle of magnetic levitation). Last but not least, a disadvantage of EPM is, that it may affect the target surface by the switching pulse in the case of target surface sensitive to current shocks [15].

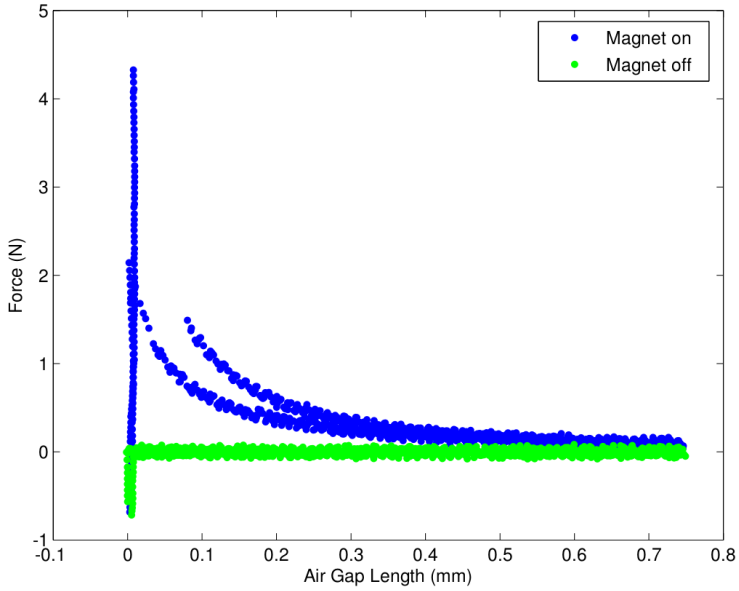

Figure 7: The dependence of the force on the size of the air gap. The data were gain from measuring dependency of the holding force on the air gap size for a miniature electropermanent magnet. This magnet was made from cylindrical rods, 1.6 mm in diameter. Courtesy of [14].

2.3.3 Practical Use of Electropermanent Magnets

The main application of the electropermanent magnets is in the cases of manipulation with heavy loads for an extended period of time or fixing the position of different mechanisms.

2.3.3.1 Grippers

Electropermanent magnets, as well as electromagnets, are widely used for manipulation of heavy loads, e.g. large iron bars or steel plates in factories. The reason why to use EPM in this kind of industrial applications is the minimal power consumption in comparison to the electromagnets and the small form factor while maintaining large forces. An example of the gripper based on the EPM is shown in Figure 8.

Another example of the EPM use are the grippers for unmanned aerial vehicles (UAVs) for gripping, carrying and moving ferrous objects. UAVs are considerably limited by the weight of the object

Figure 8: Heavy duty electropermanent magnet gripper. Courtesy of [16].

to carry due to the size and capacity of the battery that affects the action radius of the UAV. The electromagnets can be used as the grippers; however, they consume much of the battery capacity and therefore turned out to be unsuitable for such purpose. Therefore, EPMs are used for them being small and excerpt large holding forces. That means the UAVs may carry heavier objects while maintaining large operation radius because the energy from the battery is used only for a short time during the pulse switching [17]. Figure 9a shows the EPM gripper of a UAV with the joining parts to the drone which are the compression shaft and the mounting bracket. The flying UAV with the ferrous object is shown in Figure 9b.

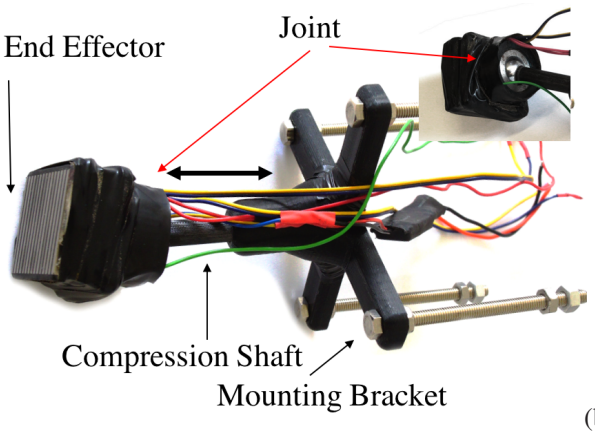

(a) The EPM gripper for UAV. Courtesy of [17].

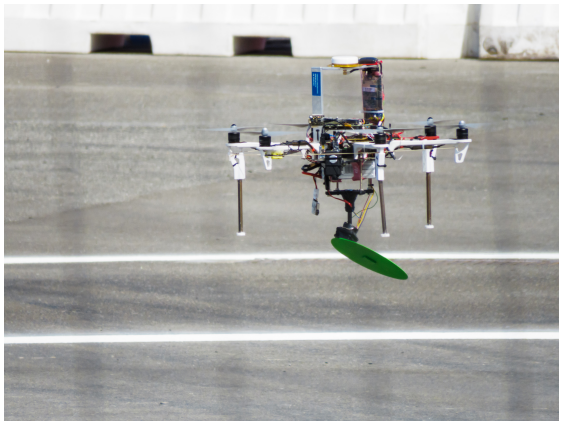

(b) UAV carrying a green ferrous object using the EPM gripper. Courtesy of [18].

Figure 9: Examples of the grippers for UAVs.

2.3.3.2 The End-points of the Climbing Robot Legs

An interesting application of the EPMs are the leg end-points of climbing robots. The problematic of climbing robots is a widely studied topic. The climbing robots are usually used for the inspection and

maintenance of the steel-made structures. Such structures include the dangerous spaces as the utility poles, oil rigs, and ship hulls. Notice, the steel structures surface conditions are rough with build-up of paint, dirt and rust, or with the presence of rivets in the older constructions.

The main and most challenging requirement for climbing robots is to move vertically and even upside down on the surface of the structures and there are few approaches described in the literature. According to [19] and [20], the adhesion methods are following: biologically inspired, electrostatic, mechanical, vacuum and magnetic. Biological inspired adhesion (micro-fibrillar based gecko feet) works on a principle of friction, but only in a single direction. Electrostatic is not suitable due to small forces, as has been already mentioned above. Mechanical adhesion can provide high holding forces; however, it typically requires more power and it is much heavier than the other forms of adhesion. The next disadvantage is a problematic movement on large flat surfaces. Further, there is the vacuum-based method, that utilize robots with sealed active suctions cups. However, the disadvantages of such a solution are the requirements for large suction power and flat, monolithic surfaces.

Magnetic adhesion appears to be the best choice for these type of robots, due to using the ferro-magnetic properties of the surfaces, although the magnetic adhesion is limited by the effective air gap due to the build-up of paint, rust and dirt as it is shown in Figure 7. All types of magnets can be used for the leg end-points of the climbing robots.

Permanent and electropermanent magnets end-points have the advantage of the failsafe system in the case of the power supply outage. The robot stays simply hanging on the construction in contrast to the electromagnetic end-points. As has been mentioned, the permanent magnets have to be pulled of mechanically or by demagnetization to lose its magnetic effect to the target surface and the electromagnets consume the power all the time when they are switched on. Therefore, it is beneficial to use the leg end-points based on the principle of EPMs [20]. Different concepts of the movement are shown in Figure 10, and they influence the used type of the magnet for the leg end-points [19].

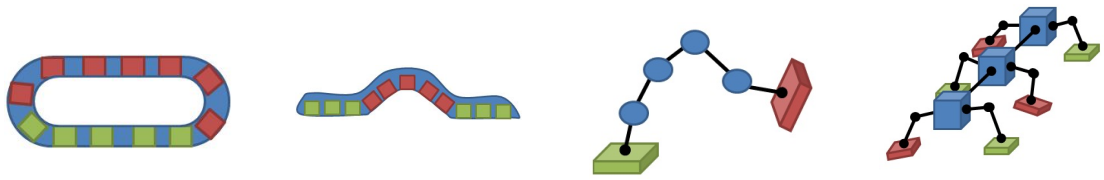

(a) Tracked concept. (b) Caterpillar concept. (c) Bipedal concept. (d) Legged concept.

Figure 10: Climbing robots movement concepts. Green color denotes the “ON” state of the EPM and the red color denotes the “OFF” state of the EPM. Courtesy of [19].

The tracked concept (Figure 10a) of the climbing robots may utilize the EPMs, but with this type of concept, the use of permanent magnets is more frequent (see Figure 11a). The magnet’s removal from the surface is due to the spinning of the wheels driving the magnetic tracks and therefore there is no need to demagnetize them.

The usage of the EPM or electromagnets is suitable for the other types of climbing robots. The bipedal climbing robot (Figure 10c) locomotes using the following principle. The EPM in the leg end-point is in the “ON” state which causes the leg holds on the surface. When the robot wants to raise the leg and make a step, the EPM is switched to the “OFF” state. Then the robot moves the leg using servo motors and the EPM is switched to the “ON” state again to stick to the surface. By repeating this procedure, the robot climbs on the surface.

The same principle applies to multi-legged robots. More legs are used for better stabilization of the climbing robot. Further, the legs can move synchronously in groups producing faster locomotion, as it is shown in Figure 10d. The practical example of the legged climbing robot is shown in Figure 11b.

The caterpillar concept (Figure 10b) of movement of the climbing robots works on the principle of activating and deactivating different segments of the flexible robot body.

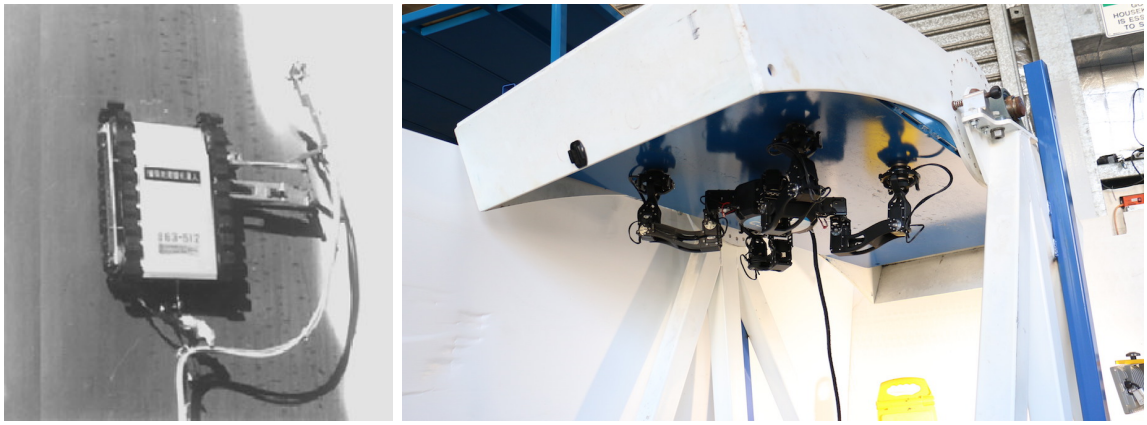

(a) The tracked climbing robot. Courtesy of [21].

(b) The legged climbing robot. Courtesy of [20].

Figure 11: Examples of climbing robots.

2.3.3.3 Connection Mechanism for Modular Robots

A self-reconfigurable modular robot is a robot, composed of a set of modules, that can change its shape by changing the connectivity of the modules. Beyond conventional actuation, sensing and control typically found in fixed-morphology robots, self-reconfiguring robots are also able to deliberately change their own shape by rearranging the connectivity of their parts, in order to adapt to new circumstances, perform new tasks, or recover from damage.

The connection between two segments can be created in different ways and it depends on the specific system. Usual approach is to use the magnetic adhesion of the modules. For example, the system M-TRAN (Modular Transformer) uses four permanent magnets for holding two modules together on each connecting surface. The module release is achieved by pulling the magnets into the module using a shape memory alloy (SMA) coil/spring linear actuator [22]. The different configurations of the modules are shown in Figure 12.

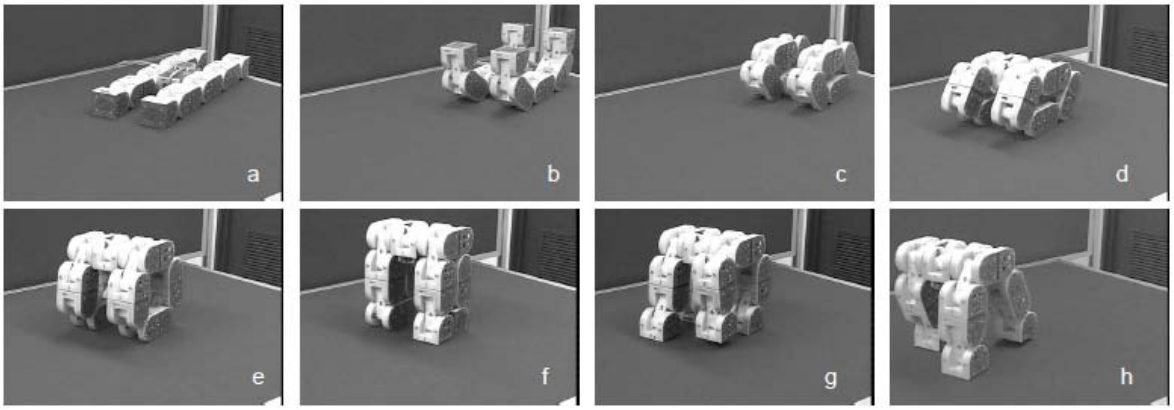

Figure 12: Different configurations of the M-TRAN modular robots. Courtesy of [22].

Modular robot system, which uses EPM for the connections of the modules, was developed at the Massachusetts Institute of Technology by Ara Nerses Knaian [14]. The modular robots are called the Robot Pebbles and they are shown in Figure 13. The Pebbles are a two dimensional, lattice-type system. The modules are cubes and pack a square grid with the edge of the module of 10 mm wide.

Each cube has four mating surfaces, each with a custom-designed electropermanent magnet connector to allow it to draw in a nearby module, mechanically bond to it, communicate, and transfer power. The electropermanent magnet connectors only require power to switch between holding states, and otherwise dissipate zero power.

Figure 14 shows the function of the modular system. In Figure 14a, there is the software design for the wanted final shape of the modules. In Figure 14b, there is realization of the shape due to EPM connections of the modules.

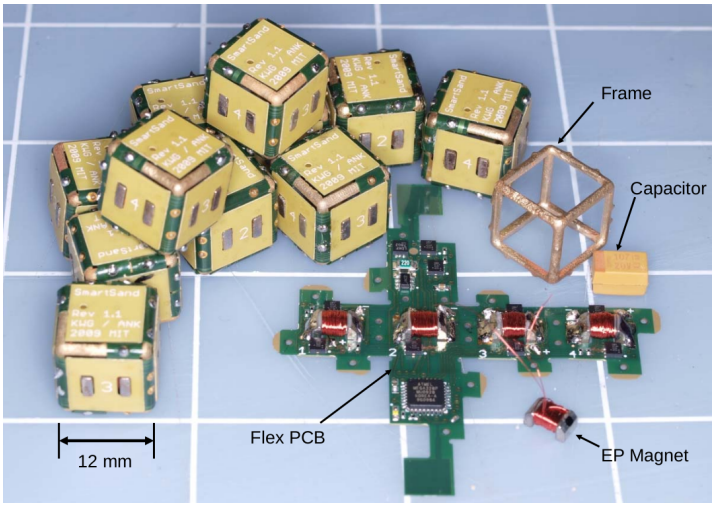

Figure 13: The Robot Pebbles. Courtesy of [14].

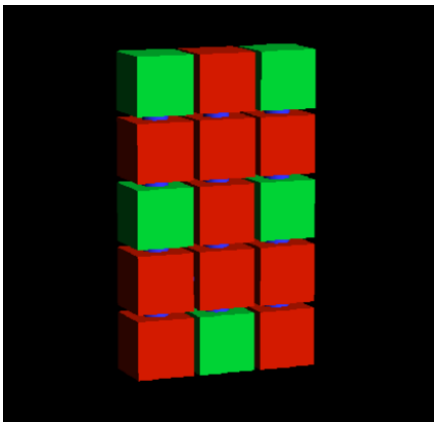

(a) Software design. Courtesy of [14].

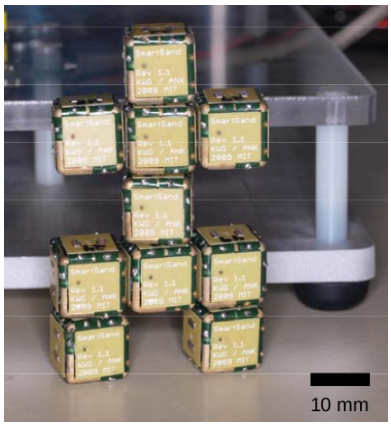

(b) Real shape made from the modules. Courtesy of [14].

Figure 14: Practical use of the Robot Pebbles. In the software design, the red cubes represent the modules which are connected. The unnecessary modules are represented by the green cubes.

2.3.3.4 Electropermanent Stepper Motor

Stepper motors can be divided according to used type of the rotor to the passive, active and hybrid. Motor is moving due to rotating magnetic field in the rotor or stator. The teeth on the rotor is tighten by teeth on the stator or vice-versa. Anyway, the motor can use magnets for switching magnetic field which makes the space for application of the EPMs which can substitute the permanent magnets. Figure 15 shows an example of a special type of an active EPM-based stepper motor. Note, this type of motor is still under the development.

The stator is cross-shaped, with an outer circular profile. The rotor has a slightly larger inner diameter and the rotor rolls around the stator in an eccentric pattern combining oscillating translation and continuous rotation [14], as it is shown in Figure 16c and Figure 16d.

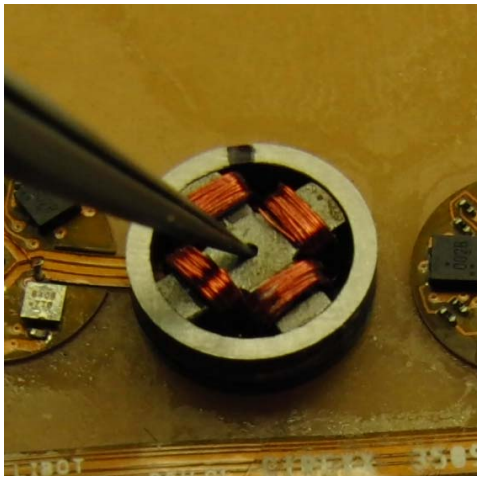

Figure 15: The EPM stepper motor. Courtesy of [14].

Figure 16 shows the principle of rotor moving of the EPM stepper motor. According to [23] the principle of the electropermanent stepper motor actuation is following. The red magnets are made from "hard" magnetic alloy and they are always polarized in the direction shown in Figure 16c and Figure 16d. The magnetization of the "soft" magnets, visualized in blue color, switches during the motor operation. The motor starts in position according to Figure 16c, with magnets 5-6 and 7-8 in "ON" state and magnets 1-2 and 3-4 in "OFF" state. Flux flows through the rotor and stator as it is shown. Applying a current pulse to the horizontal winding around magnets 5-6 and 2-1 switches the magnetization of magnets 5 and 1, turning magnet 5-6 off and magnet 2-1 on, resulting in the new flux paths shown in Figure 16d. The rotor rolls in the counterclockwise direction around magnet 7-8, taking one step to arrive at the new position. Repeated steps drives the rotor abound the stator with a continuous rotary motion and oscillating translational motion.

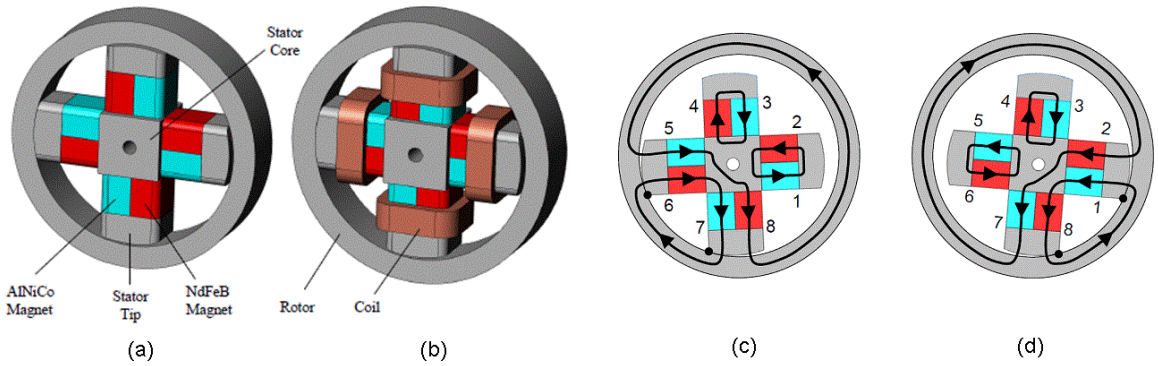

Figure 16: The EPM stepper motor principle of operation. Courtesy of [23].

2.3.3.5 Medical Applications of Electropermanent Magnets

Special anchors for instruments are used during surgical procedures, such as minimally invasive interventions in the gastrointestinal tract. Typical example is the placement of percutaneous endoscopic gastrostomy (PEG) tubes. PEG is a technique employed by surgeons to introduce an enteral feeding tube into the stomach via the abdomen. According to [24], permanent magnets represent a potential hazard during the surgery where inadvertent attraction to surgical instrumentation is often undesirable. However, it is possible to use electromagnets or EPMs, where the magnetic field can be controlled quickly and precisely, which ensures the precise manipulation with the surgical instruments.

The second application is to use the EPM for the compact magnetic resonance imaging (MRI) in dental medicine. MRI system based on an electropermanent magnet array to generate the main magnetic field is still under development [25].

2.3.3.6 Hypothetical Use of Electropermanent Magnets

Further possible use cases of the EPM can be found in the robotics field including soft robotics, origami robots or novel actuators. As has been mentioned earlier, EPM can be used as a connection mechanism in modular robotics. This principle can be further extended to soft-robots, where EPM magnets organized in polyhedron structures and submerged into the magnetic putty might be able to actuate on their own while keeping the ability to rigidly connect with other robots.

Another application of EPM might be in origami robots, that are manufactured flat and take shape after the deployment (see Figure 17). Nowadays, shape-memory alloys are mainly used as the actuators in the origami robots [26].

Last but not least, EPM might be used in novel actuators as they do not consume power when in the idle state. EPMs connected in series might form linear actuators or artificial muscle tendons. Such a tendon would be only able to shrink and would need an external force to extend; hence, the tendons would have to be used in pairs as joint flexors and extensors that cope with the biological findings.

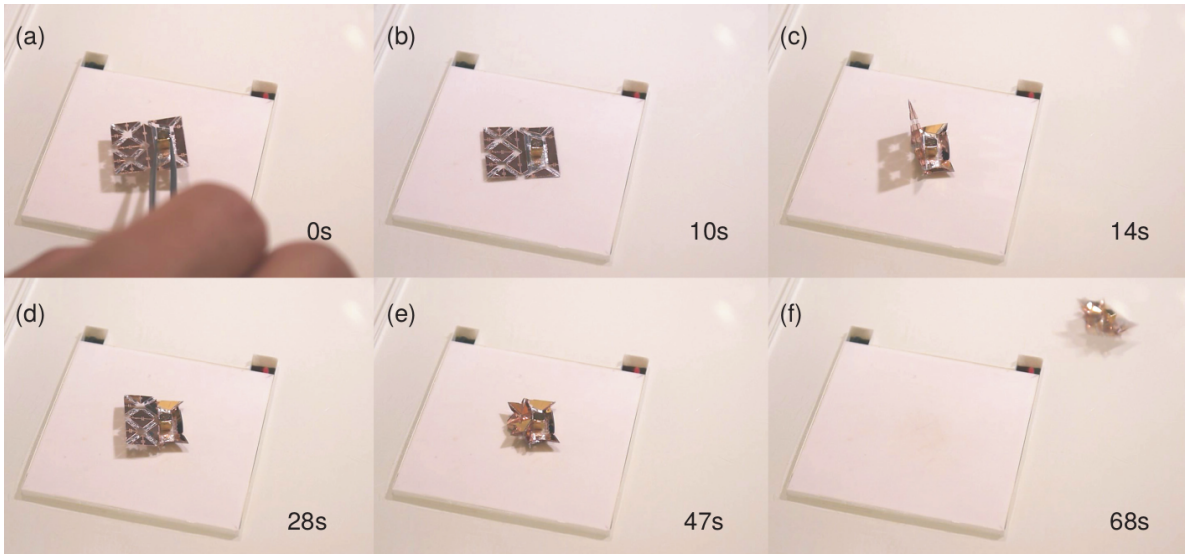

Figure 17: Self-assembly of the origami robot. Courtesy of [27]

Chapter 3
Design of Electropermanent Magnet Device

The previous chapter deals with the principle of a general electropermanent magnet. This chapter is focused on the design of the specific EPM device. Therefore, the principle of the general EPM is applied in the design of the EPM device, and the description of its real behavior is further elaborated.

The first part of this chapter is dedicated to the description of the EPM device, applying the principles of the EPM to the real device. The appropriate materials for the EPM device are mentioned as well. The second part deals with the mathematical and physical background of the EPM device. The mathematical-physical relations for the design of the EPM device are described. Based on this part, it is possible to evaluate the main parameters of the EPM device such as the dimensions of magnets and keeper bars, holding force, magnetization current, switching voltage, etc. The information and the basic equations for the next sections have been derived using description in [8, 14, 28] and [29].

Last but not least, the mathematical-physical relations have been implemented in Python and the software for parameter tuning of the EPM devices has been created.

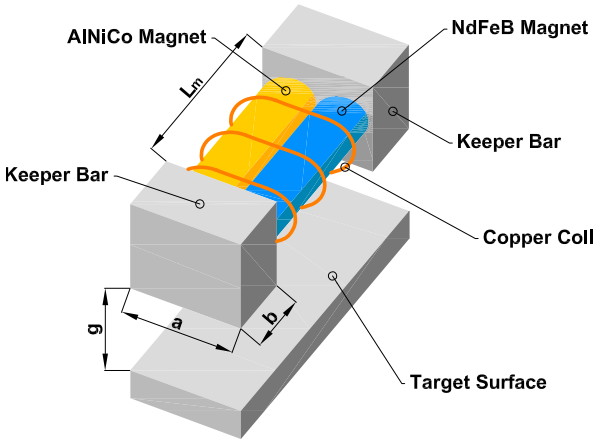

Figure 18: Visualization of the EPM device.

3.1 Operation of the Electropermanent Magnet Device

Figure 18 visualizes the EPM device. The device consists of the electropermanent magnet, the coil, and the keeper bars. The target surface is also shown in the figure. The keeper bars and the target surface are separated by an air gap. We denote the distance between the target surface and the keeper bars as g. The EPM itself consists of two magnets with almost the same remanent magnetization but with different coercivity. In this case, the Neodymium-Iron-Boron (NdFeB) magnet is used for its very high coercivity and the Aluminum-Nickel-Cobalt (AlNiCo) magnet for its low coercivity. The keeper bars and the target surface are made from iron. The coil is made from copper. Both of the magnets have the same length L_m and the diameter d.

Figure 19 shows the EPM device operation in five steps. The direction of the current is shown by red arrows, in case the current flows through the coil. The direction of the magnetic flux in the EPM device is shown by the black arrows. The individual states are illustrated by the following colors:

- Blue - switching to the "ON" state,
- Green - "ON" state,
- Magenta - switching to the "OFF" state,
- Black - "OFF" state.

The movement on the magnetic hysteresis loops of the AlNiCo and NdFeB magnet during the transition between the states is shown in Figure 19 by "working point" as the colorful points and the arrows. The loops for the AlNiCo magnet are yellow, and the loops for the NdFeB magnet are blue.

The principle of operation is following. We start with the switching "ON" state when the switching current flows through the coil in the direction which is illustrated in the first part of the figure. The AlNiCo magnet is magnetized up to the point of full saturation. The flux in the EPM device goes mainly through the EPM, but a part of the flux starts to flow through the target surface (illustrated by black interrupted lines in Figure 19). The direction of the flux in the EPM device is given by the predominant influence of the magnetic flux of the NdFeB magnet. When the AlNiCo magnet reaches the point of full saturation, the switching current is turned off. The "working point" is falling to the point where the magnetic flux density is equal to the residual magnetism. The green "working point" illustrates the "ON" state and it is shown in the second part of Figure 19. The value of the residual magnetism of the AlNiCo and the NdFeB magnet is approximately same in the "ON" state. The magnetic flux flows through the EPM device and the target surface as it is shown in the figure.

The switching current is turned on in the opposite direction when we want to turn off the EPM device. The magenta "working point" starts to fall along the magnetic hysteresis loops shown in the third part of Figure 19. For full demagnetization of the AlNiCo magnet and thus the change of the polarity of the AlNiCo magnet we want to reach the point of full saturation but in the third quadrant of the magnetic hysteresis loop. The "working point" of the NdFeB magnet fall slowly, while the "working point" of the AlNiCo magnet fall faster. Note, the "working point" of the NdFeB magnet will not cross the border of the second quadrant of its magnetic hysteresis loop. The magnetic flux is flowing mainly through the EPM magnets and the residual magnetic flux flowing through the EPM device is shown in the third part of Figure 19 by the interrupted black lines. The direction of the residual magnetic flux flowing through the EPM device is still the same due to the predominant influence of the NdFeB magnet. The switching current is turned off when the AlNiCo magnet reaches the full saturation point.

Next, the black "working point" of the AlNiCo magnet increases to the point where the magnetic flux density is equal to the negative residual magnetism. At the same time, the "working point" of the NdFeB magnet increases as well, but the black "working point" will reach the positive residual magnetism. The values of residual magnetism are approximately the same in the absolute values. Hence, the residual magnetic flux cease to flow through the target surface and the magnetic flux flows only through the magnets, hence we reach the "OFF" state of the EPM device. If we want to turn on the EPM device, the switching current has to increase in the opposite direction again.

Notice, the permanent magnets partially lose their magnetic properties during the demagnetization because some of the magnetic dipoles are not able to return to the original orientation. The AlNiCo magnet is fully magnetized and demagnetized at all times, however the "working point" of the NdFeB magnet is moving only in the first and second quadrant of the magnetic hysteresis loop. As a result, the value of the residual magnetism of the NdFeB magnet slowly falls during the EPM switching "OFF". The phenomenon is shown in Figure 20. The "working point" is creating the so-called minor loop during the movement along the magnetic hysteresis loop [28].

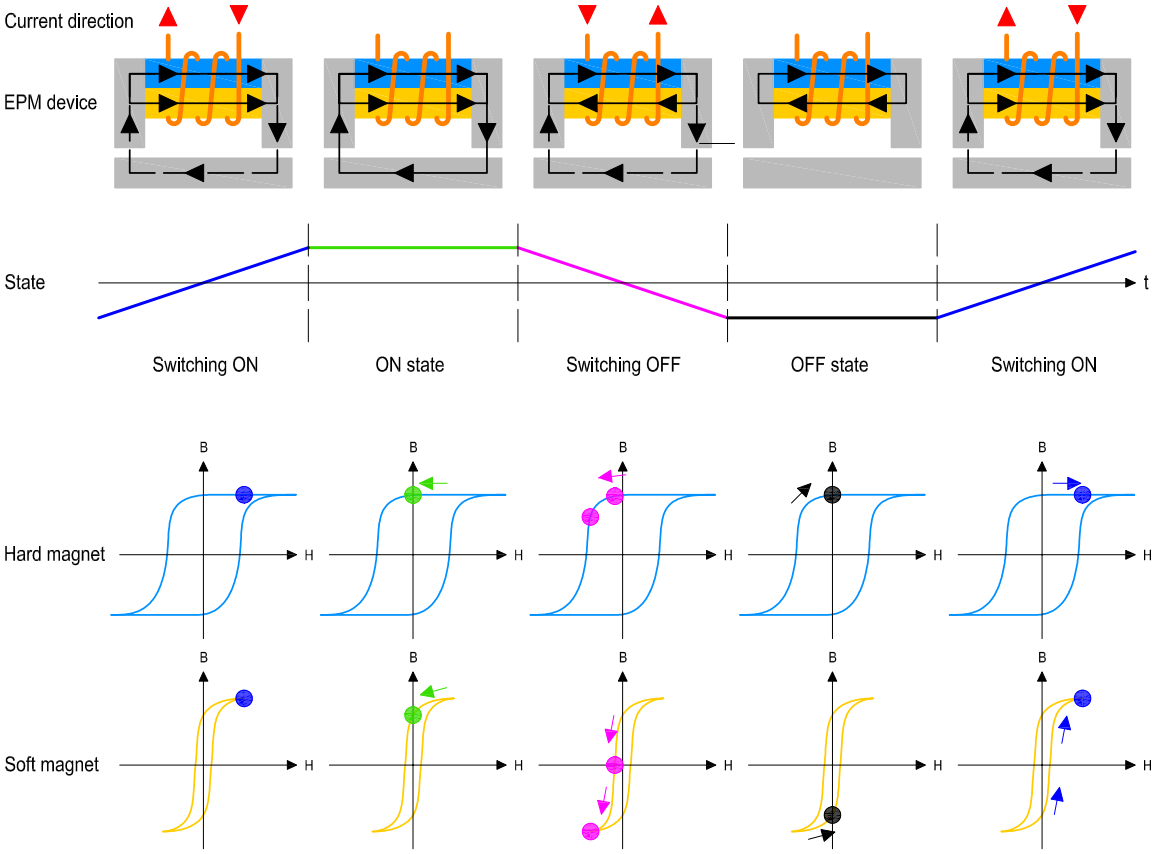

Figure 19: The EPM device operation.

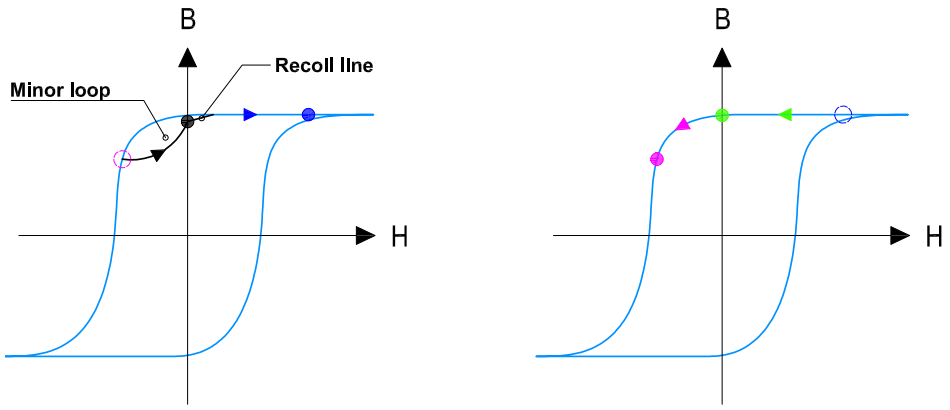

Figure 20: The minor loop of the "hard" magnetic material.

The left part of Figure 20 shows the movement of the "working point" from the switching "OFF" state to the "OFF" state when the NdFeB magnet reaches a lower value of the residual magnetism (lower by ΔB_{r}) in comparison to the previous value of the residual magnetism. On the contrary, during the transition to the "ON" state, the "working point" moves along the recoil line to reach the original saturation [28] which is visualized as the blue dot on the left side of Figure 20. When the current cease to flow through the coil, the "working point" returns back to the original value of the remanent magnetism visualized as the green dot on the right side of Figure 20.

3.2 Materials for the Electropermanent Magnet Device

It is appropriate to talk about specific materials in this chapter because their properties are the profound parameter in the design of a real EPM device. Figure 21 shows the second quadrant of "B-H curve" of the most commonly used "soft" and "hard" magnetic materials, namely Neodymium-Iron-Boron (NdFeB), Aluminum-Nickel-Cobalt 5 (AlNiCo 5), Aluminum-Nickel-Cobalt 8 (AlNiCo 8), Samarium-Cobalt (SmCo), and Ceramic 7 magnets.

The magnets from AlNiCO alloys were discovered at the beginning of the 20^{th} century and they were the strongest magnets until the 1970s when the scientists of the US Air Force Materials Laboratory discovered the properties of the rare-earth magnets, e.g. Samarium-Cobalt magnets. The difference between the AlNiCO 5 and AlNiCo 8 is mainly in the composition of the alloy and therefore their properties are different (see Figure 21 and Table 1). AlNiCo 5 consists of aluminum, nickel, cobalt, and copper in comparison to AlNiCo 8 which contains titanium in addition to these elements.

The Samarium-Cobalt materials are divided into two groups according to the composition of the alloy. The first group contains materials which are based on the alloy made from a single atom of the samarium and five atoms of the cobalt. The second group contains materials based on the alloy made from two atoms of the samarium and seventeen atoms of transition metals, which are the metals rich in cobalt, copper, and iron. The first group is used for the permanent magnets for its very high coercive force which is in order of magnitude higher than of the AlNiCo materials. The NdFeB magnets are the youngest magnets from the above mentioned - they were developed in 1982. They have higher coercivity, and they are stronger than the SmCo alloys. However, the Curie temperature of the NdFeB magnets is significantly lower than the one of the SmCo magnets (see Table 1). Ceramic materials (e.g. Ceramic 7 in Figure 21) are made from iron oxide and barium or strontium-carbonate powders and have lower residual flux densities than AlNiCo materials, but significantly higher coercive force. As a result, they are much less prone to demagnetization [28]. Now, the ceramic magnetic materials are widely used but they are not suitable for use in the EPM devices because their coercivity is too high for use in the EPM devices. Table 1 shows the values of the main parameters of all the materials mentioned above.

Table 1: Material properties of magnetic materials

Material	**Magnetic remanence** $B_\mathbf{r}$ (T)	**Coercivity** $H_\mathbf{c}$ (kA/m)	**Curie temperature** $T_\mathbf{c}$ (°C)
AlNiCo 5	1.28	51	860
AlNiCo 8	0.82	131	860
SmCo	0.8 - 1.1	600 - 2000	720 - 800
NdFeB	0.6 - 1.4	600 - 2000	320
Ceramic 7	0.2 - 0.4	100 - 300	450

The Curie temperature is one of the important parameters for choosing the material for the EPM device. The residual magnetism and the coercive force are the next parameters. Therefore, it is important to consider which magnets to use for a particular EPM device. In the case of higher temperature than 350°C, it is appropriate to use a combination of the SmCo as the "hard" magnetic material and AlNiCo 8 as the "soft" magnetic material. In the case of lower temperatures, it is appropriate to use a combination of the NdFeB as the "hard" magnetic material and AlNiCo 5 as the "soft" magnetic material.

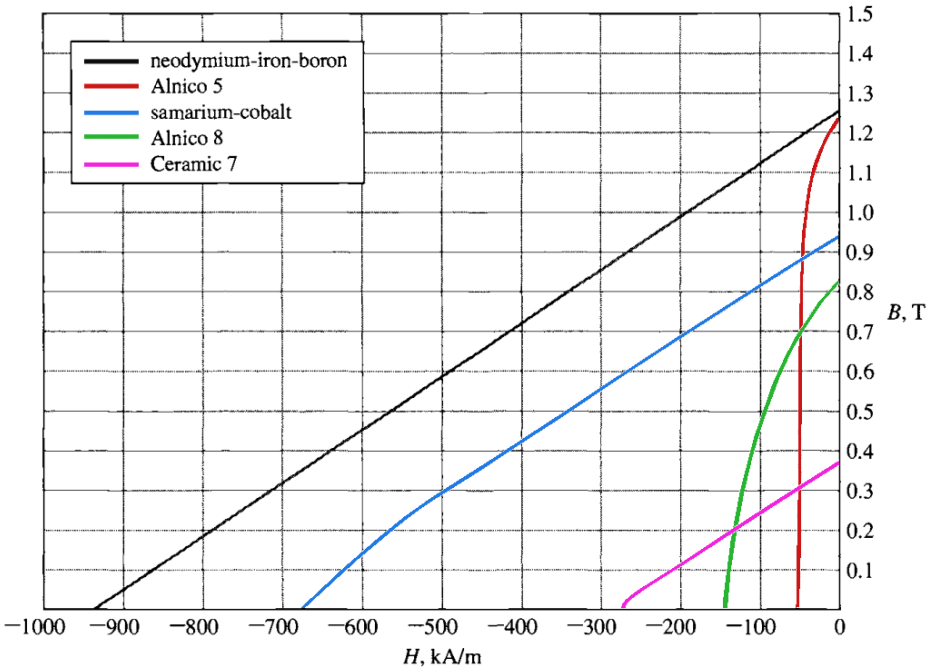

Figure 21: Magnetization curves for common permanent magnet materials. Courtesy of [28].

3.3 Equivalent Magnetic Circuit

For better understanding of EPM device behavior, it is appropriate to convert the visualization shown in Figure 18 to a magnetic circuit scheme. Figure 22 shows the equivalent magnetic circuit.

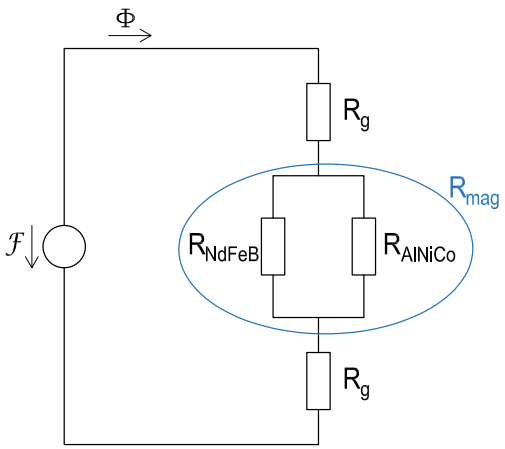

Figure 22: The magnetic circuit of the EPM device

.

In the theory of magnetic field, it is possible to use equivalent relations as in the theory of electrical field. The empiric equation for electric circuits is Ohm's law which equivalent in the theory of magnetic field is the Hopkinson's law. The Hopkinson's law describes the basic relation between the

magnetic flux Φ, magnetomotive force $\mathcal{F}$ and magnetic resistance R_{magnetic} in the magnetic circuit as:

$$\Phi = \frac{\mathcal{F}}{R_{\text{magnetic}}}.$$

It is possible to obtain the total magnetic resistance R_{tot} (in Hopkinson's law R_{magnetic}) in the same way as in the theory of electrical circuits - by sum of parallel and serial combinations of resistances. Hence, we can write:

$$R_{\text{tot}} = R_{\text{mag}} + 2R_{\text{g}}, \tag{1}$$

where R_{mag} is the parallel combination of magnetic resistance of AlNiCo magnet R_{AlNiCo} and NdFeB magnet R_{NdFeB} and R_{g} is the magnetic resistance of the air gap. The resistance of the air gap depends on the size of the air gap g, the contact area between the keeper bar and the target surface A_{g} passed by the magnetic flux, the relative permeability μ_{r}, and the vacuum permeability μ_0:

$$R_{\text{g}} = \frac{g}{\mu_0 \mu_{\text{r}} A_{\text{g}}}. \tag{2}$$

The resistances of the AlNiCo magnet R_{AlNiCo} and the NdFeB magnet R_{NdFeB} depend on their material properties that are represented by the relative permeability μ_1 and μ_2 respectively, and the length of magnets L_{m} and their area A_{m}:

$$R_{\text{AlNiCo}} = \frac{L_{\text{m}}}{\mu_0 \mu_1 A_{\text{m}}}, \tag{3}$$

$$R_{\text{NdFeB}} = \frac{L_{\text{m}}}{\mu_0 \mu_2 A_{\text{m}}}. \tag{4}$$

Given the above relations, we can write:

$$R_{\text{mag}} = \frac{R_{\text{AlNiCo}} \cdot R_{\text{NdFeB}}}{R_{\text{AlNiCo}} + R_{\text{NdFeB}}} = \frac{\frac{L_{\text{m}}}{\mu_0 \mu_1 A_{\text{m}}} \cdot \frac{L_{\text{m}}}{\mu_0 \mu_2 A_{\text{m}}}}{\frac{L_{\text{m}}}{\mu_0 \mu_1 A_{\text{m}}} + \frac{L_{\text{m}}}{\mu_0 \mu_2 A_{\text{m}}}}. \tag{5}$$

The final relation for R_{mag} given the simplification $\mu = \mu_0 (\mu_1 + \mu_2)$ is:

$$R_{\text{mag}} = \frac{L_{\text{m}}}{\mu A_{\text{m}}}. \tag{6}$$

The final relation for the total magnetic resistance of the circuit is:

$$R_{\text{tot}} = \frac{L_{\text{m}}}{\mu A_{\text{m}}} + \frac{2g}{\mu_0 \mu_{\text{r}} A_{\text{g}}}. \tag{7}$$

Further, the relation for the magnetomotive force, which is the cause of the magnetic flux in the circuit, is following:

$$\oint_l \boldsymbol{H}\, \mathrm{d}\mathbf{l} = \sum I = N_{\text{turn}} I = \mathcal{F}, \tag{8}$$

where $\boldsymbol{H}$ is the magnetic field intensity, $\mathrm{d}\mathbf{l}$ is the length element, N_{turn} is the number of winding turns and I is the current of the copper coil.
For the total magnetic flux which flows through the magnetic circuit it is possible to write:

$$\Phi = \frac{N_{\text{turn}} I}{\frac{L_{\text{m}}}{\mu A_{\text{m}}} + \frac{2g}{\mu_0 \mu_{\text{r}} A_{\text{g}}}}. \tag{9}$$

3.4 Parameters of the Electropermanent Magnet Device

This section describes the individual characteristics of the EPM device, such as the switching current, the switching voltage, the holding force, etc., which are necessary for proper design and simulation of the EPM device.

3.4.1 Force

The holding force is the crucial parameter of the EPM device. It affects, among other things, the geometry of the device as will be shown below.

3.4.1.1 Flux Equations

First, it is necessary to realize that due to the Gauss's law for magnetism, the magnetic flux in magnetic circuits always forms closed loops. If we use this idea for our EPM device and we imagine that the magnetic flux goes through the device in the "ON" state from the magnets to the first keeper bar, through the air gap to the target surface, then it continues through the second air gap to the second keeper bar and again to the magnets, there is nowhere (in the ideal case) where the magnetic flux can dissipate. In the real case, even when the size of the air gaps approaches zero, there will be still losses due to the material imperfections between the keeper bars and the target surface given by the material properties. Therefore, the "pole-to-pole" leakage flux Φ_{leak} appears in the magnetic circuit. It represents the losses in the materials or in the air gap and it is described by the relations below. First, we start with the following equation:

$$\Phi_{\text{m}} = \Phi_{\text{g}} + \Phi_{\text{leak}}, \tag{10}$$

where Φ_{m} is the magnetic flux through the magnets and Φ_{g} is the magnetic flux through the air gap.

The basic relation between the magnetic flux Φ, magnetic flux density B and the area passed by magnetic flux A is denoted as:

$$\Phi = BA, \tag{11}$$

By combining equations (10) and (11) it is possible to write:

$$B_{\text{m}}A_{\text{m}} = B_{\text{g}}A_{\text{g}} + \Phi_{\text{leak}}, \tag{12}$$

where B_{m} is the axial magnetic flux density in material of used magnets, A_{m} is the area of the magnets, B_{g} is the axial magnetic flux density in the air gap and A_{g} is the area of the keeper bar which belongs to the air gap.

In this case, the axial magnetic flux density is given by combination of AlNiCo and NdFeB materials as:

$$B_{\text{m}} = B_{\text{AlNiCo}} + B_{\text{NdFeB}}, \tag{13}$$

where B_{AlNiCo} is the axial magnetic flux density in AlNiCo and B_{NdFeB} is the axial magnetic flux density in NdFeB. The area of the used magnets with circular cross section is:

$$A_{\text{m}} = \frac{\pi d^2}{4} N_{\text{rods}}, \tag{14}$$

where d is the diameter of the magnet and N_{rods} is the number of used magnets which does not depend on the used material of magnets. The area of the keeper bar adjacent to the air gap is simply $A_{\text{g}} = ab$, where a and b are the dimensions of the keeper bar (see Figure 18).

The equations above yield:

$$\left(B_{\text{AlNiCo}} + B_{\text{NdFeB}}\right) \frac{\pi d^2}{4} N_{\text{rods}} = B_{\text{g}} ab + \Phi_{\text{leak}}. \tag{15}$$

Based on equation (8) it is possible to write:

$$H_{\text{m}} L_{\text{m}} + 2 H_{\text{g}} g = N_{\text{turn}} I = \mathcal{F}, \tag{16}$$

where H_{m} is the axial magnetic field intensity of either of the magnets, L_{m} is the length of the magnets, H_{g} is the axial magnetic field intensity in the air gap and the dimension between the target surface and the keeper bar is g.

Next, the expression for axial magnetic flux has to be derived to get the equation for the holding force. According to the magnetization characteristics in Figure 21 it is possible to write individual axial magnetic flux densities in individual materials as:

$$B_{\text{g}} = \mu_0 H_{\text{g}}, \tag{17}$$

$$B_{\text{NdFeB}} = B_r + \mu_r H_{\text{m}}, \tag{18}$$

$$B_{\text{AlNiCo}} = B_{\text{AlNiCo}} \left(H_{\text{m}} \left(t\right), t\right), \tag{19}$$

where μ_r is the relative permeability and B_r is the remanent magnetization.

Notice, the dependency of the B_{NdFeB} on H_{m} is linear, whereas the dependency of the B_{AlNiCo} on H_{m} is nonlinear, which can be observed in the BH diagram shown in Figure 21. Therefore, equations (18) and (19) are given *as is*.

The equation for the estimation of the flux, that flows through the EPM device, can be derived by substituting (17), (18) and (19) into (15):

$$\left(B_r + \mu_r H_{\text{m}} + \left(B_{\text{AlNiCo}} H_{\text{m}}(t), t\right)\right) \frac{\pi}{4} d^2 N_{\text{rods}} = B_{\text{g}} ab + \Phi_{\text{leak}}. \tag{20}$$

The last unknown member of the equation (20) is the leakage flux Φ_{leak}. It is difficult to calculate the leakage flux directly, but it is possible to estimate its value based on the leakage coefficient, which expresses the value of the reduction of the main magnetic flux. It means the leakage flux does not participate on the main magnetic flux. Then we can use the equation (16) and given the leakage permeance P_{leak} (the leakage permeance is defined as the inverse of magnetic reluctance), it is possible to write the equation:

$$H_{\text{m}} L_{\text{m}} + \frac{\Phi_{\text{leak}}}{P_{\text{leak}}} = N_{\text{turn}} I. \tag{21}$$

Then the leakage flux is denoted as:

$$\Phi_{\text{leak}} = \left(N_{\text{turn}} I - H_{\text{m}} L_{\text{m}}\right) P_{\text{leak}}. \tag{22}$$

The final equation for description of the flux in the EPM device is given by the combination of the equations (20) and (22):

$$\left(B_r + \mu_r H_{\text{m}} + \left(B_{\text{AlNiCo}} H_{\text{m}}(t), t\right)\right) \frac{\pi}{4} d^2 N_{\text{rods}} = \left(N_{\text{turn}} I - H_{\text{m}}(t) L_{\text{m}}\right) \left(\frac{\mu_0 ab}{2g} + P_{\text{leak}}\right). \tag{23}$$

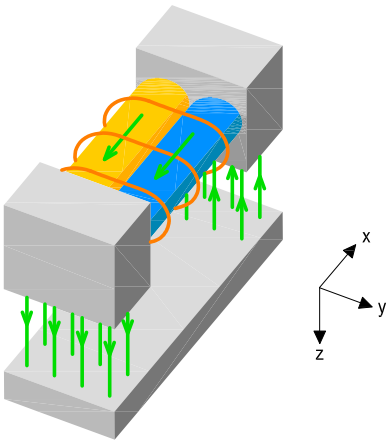

Figure 23: The direction of the magnetic flux flowing through the EPM device. The direction is shown by the green arrows. Notice, the magnetic flux flowing parallel with the axis z between the keeper bar and the air gap.

3.4.1.2 Maxwell Stress Tensor

The magnetic flux flows through the device from the magnets to the first keeper bar, then through the air gap to the target surface, then it continues through the second air gap to the second keeper bar and again to the magnets, as has been written above. The main flux is perpendicular to the surface of the keeper bar near the gap as it is shown in Figure 23. Henceforth, the force per area is given by the σ_{zz} component of the Maxwell stress tensor.

The components σ_{ij} of the Maxwell stress tensor for magnetic field in vacuum are defined as:

$$\sigma_{ij} = \frac{1}{\mu_0} B_i B_j - \frac{1}{2\mu_0} B^2 \delta_{ij}, \tag{24}$$

where B_i, B_j are flux densities and δ_{ij} is the Kronecker's delta. Kronecker's delta is a function of two variables given as:

$$\delta_{ij} = \begin{cases} 1 & \text{for} \quad i = j, \\ 0 & \text{otherwise.} \end{cases}$$

In this case, when we will use only σ_{zz}, the Maxwell stress tensor is:

$$\sigma_{zz} = \frac{1}{2\mu_0} B_{\mathrm{g}}^2. \tag{25}$$

The force F is given from Maxwell stress tensor as:

$$F = \sigma_{zz} A_{\mathrm{g}} = \frac{B_{\mathrm{g}}^2 ab}{\mu_0}. \tag{26}$$

The final equation for the force can be derived by substituting (16) and (17) into (26):

$$F = ab \frac{\mu_0}{4} \left(\frac{N_{\mathrm{turn}} I - H_{\mathrm{m}} L_{\mathrm{m}}}{g} \right)^2. \tag{27}$$

3.4.1.3 Holding Force

In order to evaluate the magnitude of the holding force of the real EPM device we have to introduce a few simplifying assumptions. The following are the simplifying assumptions.

- The AlNiCo magnet and NdFeB magnet are fully magnetized in the same direction.
- The magnetic flux density of AlNiCo magnet and NdFeB magnet are equal, in the "ON" state and in the "OFF" state with the inverted sign, according to Figure 19, and it applies:

$$B_{\text{AlNiCo}} = B_{\text{NdFeB}} = B_r.$$

- The length of the air gap is equal to zero.
- The leakage flux is zero due to $g \to 0$.

Then, it is possible to simplify equation (15) to the form:

$$B_{\text{g}} = \frac{\pi}{4ab} d^2 N_{\text{rods}} B_r. \tag{28}$$

The holding force F_{H} is given by the combination of equations (26) and (28):

$$F_{\text{H}} = \frac{1}{\mu_0 ab} \left(\frac{\pi d^2 N_{\text{rods}} B_r}{4} \right)^2. \tag{29}$$

Notice, the holding force will increase, with the assumption $\Phi = \text{const.}$, if the area ab of the keeper bar is reduced.

We want to maximize the holding force. Therefore, the keeper bars are made from the ferromagnetic material. However, the ferromagnetic material, in our case the iron, has a property known as the magnetic saturation, where any further increase in the applied external magnetic field cannot increase the magnetic flux density of that material. It means that the magnetic flux density of the keeper bar B_{g} has to be equal to maximal magnetic saturation B_{sat} of the material or lower. Then it is possible to denote the maximal holding force F_{Hmax} according to the equation (26) as:

$$F_{\text{Hmax}} = \frac{B_{\text{sat}}^2 ab}{\mu_0}. \tag{30}$$

3.4.2 Coil Resistance

It is necessary to determine the coil resistance to determine the voltage and the switching current. The coil resistance is equal to the resistance of an unrolled wire. The cross-section of the coil with the basic dimensions is depicted in Figure 24.

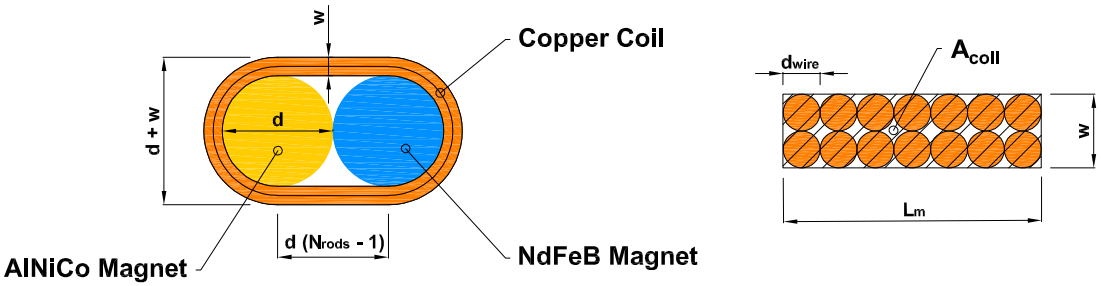

Figure 24: Cross-section of the coil.

The coil resistance R_{coil} is defined as:

$$R_{\text{coil}} = \rho \frac{l_{\text{wire}}}{A_{\text{wire}}}, \tag{31}$$

where ρ is the specific electrical resistance, l_{wire} is the length of the unrolled wire and A_{wire} is the area of the wire. Equations for the A_{wire} and l_{wire} according to Figure 24 are following:

$$A_{\text{wire}} = \frac{\pi d_{\text{wire}}^2}{4}, \tag{32}$$

$$l_{\text{wire}} = N_{\text{turn}} \left[2d(N_{\text{rods}} - 1) + \pi \left(d + w\right)\right], \tag{33}$$

where d_{wire} is the diameter of the wire, N_{turn} is the number of the coil turns and w is the height of the coil. With the simplifying assumption that the cross-section of the coil has a shape of a rectangle according to Figure 24, it is possible to denote the cross-section area of the coil A_{coil}:

$$A_{\text{coil}} = N_{\text{turn}} d_{\text{wire}}^2 = L_{\text{m}} w. \tag{34}$$

The final relation for the coil resistance can be obtained by expressing d_{wire} from (34) and substituting it into equation (33) as:

$$R_{\text{coil}} = \frac{4\rho N_{\text{turn}}^2}{L_{\text{m}}} \left[\frac{d}{w}\left(\frac{2N_{\text{rods}} - 2}{\pi} + 1\right) + 1\right]. \tag{35}$$

3.4.3 Current

For the change of the state of the EPM device into the "ON" state, it is necessary to apply a voltage pulse to the coil, until the coil current rises to I_{max}. Due to this process, the direction of the flux in AlNiCo magnet is the same as the direction of the flux in the NdFeB magnet, thus the EPM device can hold the target surface as described above. The required current to revert the flux in the AlNiCo magnet is given by the solution of equation (23) for the current. We get the following relation, with the notice that the AlNiCo magnet need to reach saturation (the indices of H_{m} and B_{m} will change to H_{ms} and B_{ms}):

$$I_{\text{max}} = \frac{H_{\text{ms}} L_{\text{m}}}{N_{\text{turn}}} + \frac{\pi d^2 N_{\text{rods}} \left(B_{\text{ms}} + B_r + \mu_0 H_{\text{ms}}\right)}{8N_{\text{turn}} \left(\frac{\mu_0 ab}{2g} + P_{\text{leak}}\right)}. \tag{36}$$

Notice, the dependence of the I_{max} on the length is linear. Given the simplifying assumptions described in Section 3.4.1.3 it applies:

$$I_{\text{max}} = \frac{H_{\text{ms}} L_{\text{m}}}{N_{\text{turn}}}. \tag{37}$$

3.4.4 Voltage

The remagnetization of the AlNiCo magnet is achieved by applying a pulse of the switching voltage V to the coil that is strong enough to cause reorganization of the magnetic domains in the AlNiCo magnet. The voltage drop in the coil is time dependent and it is given by the Faraday's law and Ohm's law as:

$$V\left(t\right) = N_{\text{turn}} \left(\frac{dB_{\text{AlNiCo}}}{dt} + \frac{dB_{\text{NdFeB}}}{dt}\right) \frac{\pi d^2 N_{\text{rods}}}{8} + I\left(t\right) R_{\text{coil}}. \tag{38}$$

Equation (38) models the complex nonlinear electrical response of the EPM device and can be solved numerically. However, a valuable constraint on the minimum switching voltage V_{min} can be derived using the following intuition.

Notice, equation (38) has two parts. First part describes the voltage drop caused by remagnetization of the AlNiCo magnet, whereas the second part is voltage drop in the coil caused by material properties of the coil. If the derivation d/dt of the first member of the equation equals zero we get only the voltage drop in the coil V_{coil} which corresponds to the state in which the magnetic flux is close to the saturation limit; i.e. if the switching voltage in the coil will be lower than the V_{coil} we will not be able to ensure the current flow through the coil, which will prevent the remagnetization of the AlNiCo magnet. Therefore, the minimum switching voltage has to be higher than the V_{coil}. Hence, given the $d/dt = 0$ we obtain relation for calculation of the minimum voltage V_{min} as:

$$V_{\text{min}} = I_{\text{max}} R_{\text{coil}}. \tag{39}$$

The final equation for the required voltage can be derived by substituting (36) and (35) into (39):

$$V_{\text{min}} = \rho N_{\text{turn}} \left[4H_{\text{ms}} + \frac{\pi d^2 N_{\text{rods}} \left(B_{\text{ms}} + B_r + \mu_0 H_{\text{ms}} \right)}{2L_{\text{m}} \left(\dfrac{\mu_0 ab}{2g} + P_{\text{leak}} \right)} \right] \left[\frac{d}{w} \left(\frac{2N_{\text{rods}} - 2}{\pi} + 1 \right) + 1 \right]. \tag{40}$$

Given the simplifying assumptions described in Section 3.4.1.3, it is possible to rewrite the equation above to:

$$V_{\text{min}} = 4\rho N_{\text{turn}} H_{\text{ms}} \left[\frac{d}{w} \left(\frac{2N_{\text{rods}} - 2}{\pi} + 1 \right) + 1 \right]. \tag{41}$$

3.4.5 Inductance

Inductance L is the next important parameter of the EPM device because it is necessary to evaluate the inductance for the calculation of the switching time T. The basic relation for the inductance is given as:

$$L = \frac{\Phi}{I}, \tag{42}$$

after the substitution:

$$L = \frac{\pi d^2 N_{\text{turn}} N_{\text{rods}} \left(B_{\text{ms}} + B_r + \mu_0 H_{\text{ms}} \right)}{8 I_{\text{max}}}. \tag{43}$$

By the combination of the equations (36) and (43) we get the equation for the inductance:

$$L = N_{\text{turn}}^2 \left[\left(\frac{\mu_0 ab}{2g} + P_{\text{leak}} \right)^{-1} + \left(\frac{\pi d^2 N_{\text{rods}} \left(B_{\text{ms}} + B_r + \mu_0 H_{\text{ms}} \right)}{8 L_{\text{m}} H_{\text{ms}}} \right)^{-1} \right]^{-1}. \tag{44}$$

We use the simplifying assumptions from Section 3.4.1.3, again. The final relation for the inductance is following:

$$L = N_{\text{turn}}^2 \left(\frac{\pi d^2 N_{\text{rods}} \left(B_{\text{ms}} + B_r + \mu_0 H_{\text{ms}} \right)}{8 L_{\text{m}} H_{\text{ms}}} \right). \tag{45}$$

3.4.6 Length of the switching pulse

The EPM device can be considered as a series LR circuit. Then it applies:

$$I(t) = \frac{V}{R} \left(1 - e^{-\dfrac{t}{\tau}} \right), \tag{46}$$

where τ is the time constant and $\tau = L/R$ in general. The function above is monotonically increasing which means that it is possible to write:

$$I_{\text{max}} = \frac{V}{R}\left(1 - e^{-\frac{T}{\tau}}\right). \tag{47}$$

The solution for the T (the pulse length) is gained by the combination of the relations (39) and (47)

$$T = \tau \ln\left(\frac{V}{V - V_{\text{min}}}\right), \tag{48}$$

where $\tau = L/R_{\text{coil}}$ in this case.

3.4.7 Parameters Summary

The basic physical quantities were derived in six previous sections. Table 2 summarizes the basic parameters and the basic relations among them in the simplified form, given the assumption that the air gap is zero. Nevertheless, the derived set of equations gives us a tool to easily find parameters of the EPM device and estimate its performance. Such an insight is very important prior the demanding numerical simulation of the EPM behavior and the fabrication of the EPM device.

Table 2: EPM device basic parameters

Parameter	**Symbol**	**Units**	**Equation**
Holding force	F_{H}	N	$F_{\text{H}} = \frac{1}{\mu_0 ab}\left(\frac{\pi d^2 N_{\text{rods}} B_r}{4}\right)^2$
Coil Resistance	R_{coil}	Ω	$R_{\text{coil}} = \frac{4\rho N_{\text{turn}}^2}{L_{\text{m}}}\left[\frac{d}{w}\left(\frac{2N_{\text{rods}} - 2}{\pi} + 1\right) + 1\right]$
Current	I_{max}	A	$I_{\text{max}} = \frac{H_{\text{ms}} L_{\text{m}}}{N_{\text{turn}}}$
Voltage	V_{min}	V	$V_{\text{min}} = 4\rho N_{\text{turn}} H_{\text{ms}}\left[\frac{d}{w}\left(\frac{2N_{\text{rods}} - 2}{\pi} + 1\right) + 1\right]$
Inductance	L	H	$L = N_{\text{turn}}^2\left(\frac{\pi d^2 N_{\text{rods}}\left(B_{\text{ms}} + B_r + \mu_0 H_{\text{ms}}\right)}{8 L_{\text{m}} H_{\text{ms}}}\right)$
Pulse Length	T	s	$T = \tau \ln\left(\frac{V}{V - V_{\text{min}}}\right)$

3.5 Elecropermanent Magnet Parameterization Using Python Model

The mathematical-physical relations described in Section 3.4 have been implemented in the programming language Python to visualize the dependencies of the aforementioned parameters and to help with finding the parametrization of the real EPM device. The developed software model consists of two parts. First part consists of sliders that make it possible to change the individual parameter values. The second part shows graphs of the dependent quantities. The user interface with sliders is visualized in Figure 25 and the resulting graphs are depicted in Figure 26.

The graphs in Figure 26 visualize the general dependencies of the quantities for the given parameters (blue and orange lines) and the exact value for the particular input (red points) given by the sliders. The graphs shows the four main dependencies of the parameters - the dependence of the holding force F_{H} and maximal holding force F_{Hmax} on the keeper bar area A, the dependence of the holding force F_{H} on the magnets diameter d, the dependence of the maximal current I_{max} value on the number of the coil turns N_{turn} and the dependence of the pulse length T on the voltage V. Notice, e.g., for the parametrization of the EPM device given by Figure 25 the value of the holding force is 182.7 N, i.e., the EPM device can hold more than 18 kg. However, the graphs show the theoretical values of the parameters. It is necessary to take into account further influencing factors, e.g. leakage flux, for the more accurate values of the parameters of the EPM device which could be done using a realistic simulation described in Section 4.

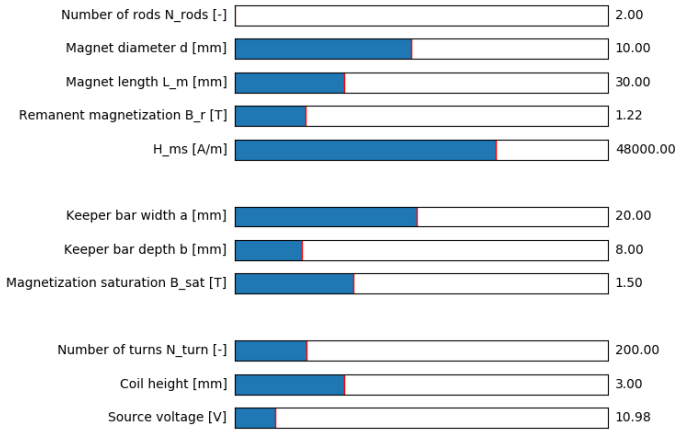

Figure 25: The parametrization interface of the Python simulation.

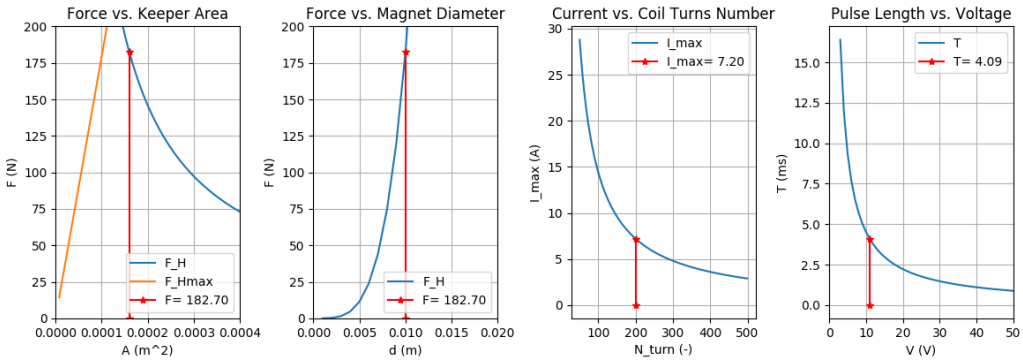

Figure 26: The graphs of the parameters dependencies.

3.5.1 Design of the Real Electropermanent Magnet Device

For the purpose of the design and manufacture of the real EPM device, it is necessary to determine the material properties and the dimensions of the EPM device first. Next, the EPM device parameters will be used for the detailed simulation and for the experimental evaluation on the real EPM device. By using the developed simplified model in Python which is described in Section 3.5 a particular parametrization has been determined, that respects constraints ensuring the manufacturability of the real EPM. The particular constraints include dimensions constrains imposed by the manufacturers of the NdFeB and AlNiCo magnets, the dimensions of the keeper bars, admissible switching voltages and currents, and the user-defined requirements on the holding force.

The EPM device parametrization has been selected such as the device should be able to excerpt the holding force of approximately 10 N. The resulting parametrization given by the device dimensions and the material properties that has been used with the simulation and the manufacturing of the real EPM device is listed in Table 3. Figure 27 shows the expected values of the dependent parameters which are calculated by the software in Python. The expected holding force F_{H} is 14.97 N, the maximal current I_{max} for the magnetization and demagnetization of the AlNiCo magnet is 4.8 A when the coil has 100 turns. The switching pulse length T should be at least 0.3 ms given the power source voltage V of 12 V.

Table 3: EPM device properties

Parameter	Symbol	Value	Units
Keeper bar length	a	10	mm
Keeper bar width	b	5	mm
Magnet diameter	d	4	mm
Magnet length	L_{m}	10	mm
Number of the rods	N_{rods}	2	-
Number of the coil turns	N_{turn}	100	-
Remanent magnetization	B_{r}	1.22	T
Magnetic saturation	B_{sat}	1.5	T
Coercivity	H_{ms}	48	kA/m

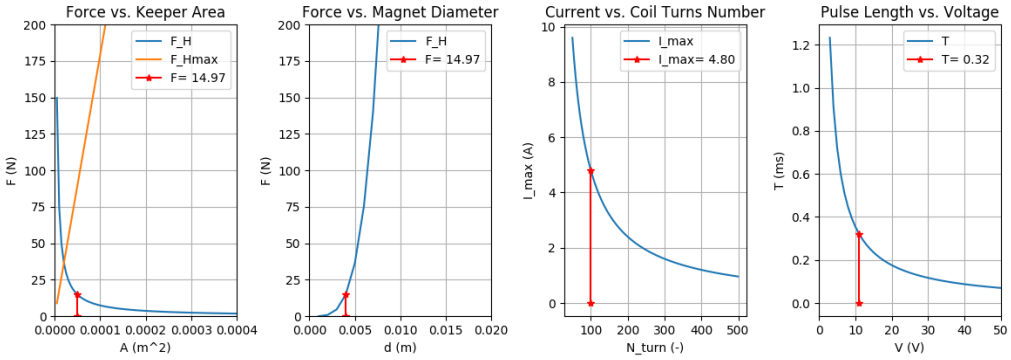

Figure 27: Real EPM device parameters dependencies.

Chapter 4
Simulation and Experimental Results

The theoretical design of electropermanent magnet device has been presented in the previous chapter. The simulations in the software ANSYS Maxwell are described in this chapter together with the verification of the theoretical knowledge of the real EPM device. The goal of this chapter is to verify the value of the holding force calculated in Section 3.5.1 in simulation and experimentally with the real EPM device. Further, the purpose of the simulation is to prove that the direction of the magnetic flux is really changed in the "ON" state and "OFF" state of the EPM device and the course of the magnetic flux corresponds with the theoretical part of this thesis.

4.1 ANSYS Maxwell

The software ANSYS Maxwell has been used for the simulations [30] of the real EPM device which supports simulations of the low frequency electromagnetic fields. The ANSYS Maxwell uses solvers for the electromagnetic static and transient events, and therefore it is often used for modeling and simulation of the electric motors, generators, transformers, and other electromagnetic devices. The solvers of the software are based on the Finite Element Method (FEM).

4.1.1 Finite Element Method

The FEM is used for the numerical solution of complex problems. Typically, these problems include structural, fluid flow, heat transfer, and electromagnetic analysis. The most of the mathematical-physical phenomena is possible to describe using systems of partial differential equations, however, the boundary conditions for these equations are not easily to be found. Therefore the analytic solution is very complicated or impossible for the general areas.

The main principle of the FEM is that the general area is divided into smaller areas, called finite elements. The FEM uses the system of basic algebraic equations to describe these areas. The simple equations that model these finite elements are then assembled into a larger system of equations that models the entire problem. The FEM then uses variational methods from the calculus of variations to approximate a solution by minimizing an associated error function [31], [32] by iterative refinement of the solution.

4.1.2 Simulation Setup

The EPM device used for the simulation has been modeled according to the specifications described in Section 3.5.1. In particular, the dimensions and the material properties for simulation are given in Table 3. Figure 28a shows the model of the EPM prepared for the simulation. The colors of the EPM device parts in ANSYS Maxwell corresponds to the visualizations of the EPM device in Chapter 3.

Figure 28b shows the mesh plot of the EPM device divided into smaller areas used for the calculation of FEM, as it is mentioned in Section 4.1.1.

The magnetostatic and transient solvers have been used for the simulation of the EPM with the following analyzer parametrization:

- Percent error - 1%,
- Maximum number of passes - 10,

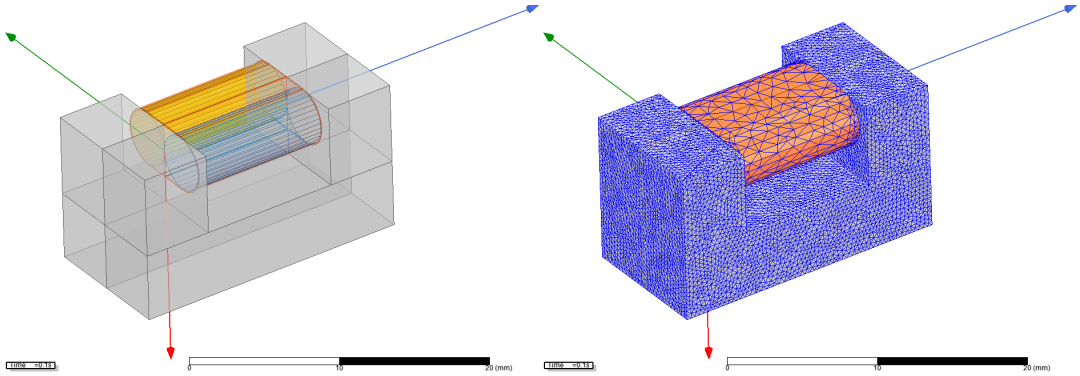

(a) The EPM device model with the target surface for the simulation.

(b) The mesh plot of the EPM device model with the target surface.

Figure 28: The EPM device model with the target surface for the simulation.

- Minimum number of passes - 2,
- Stop time - 0.1 s,
- Time step - 2 ms.

The *Percent error* represents the measure of solution convergence of the solver and it is reported after each solution pass, hence, it is desirable to set this value low to ensure quality solution. However, low values of *Percent error* impose significant computational requirements and usually large number of passes is necessary. The number of passes can be limited regardless the solution quality by *Maximum number of passes* and *Minimum number of passes* parameters as the upper bound and lower bound of the number of passes respectively. Further, the *Stop time* and *Time step* are necessary parameters for the transient solver. They represent the overall simulation time and the time step with which the simulation is computed.

4.1.3 Simulation Results

One purpose of the simulations has been to prove that the magnetic flux direction is really changed in the "ON" state and "OFF" state of the EPM device and that the magnetic flux corresponds with the theoretical part of this thesis. Two individual simulations have been performed with the altering magnetization of the AlNiCo magnet. The results of the simulation, which prove the changing direction of the magnetic flux in the device, are shown in Figure 29. The figure shows the simulated vectors of magnetic flux density which, in effect, shows the changes in the magnetic flux.

Figure 30 shows the individual orthogonal views of the EPM device model. The left column of Figure 30 shows the plots of the EPM in "ON" state, while the right column shows the plots of the EPM in "OFF" state. From top to bottom the individual figures show left side, top, bottom and right side views respectively.

The simulated results cope with the herein derived theory. In "ON" state, the magnetic flux flows through the magnets to the keeper bars and through the target surface. In "OFF" state, the majority of the magnetic flux flows only through the magnets and keeper bars. Note, a fraction of the magnetic flux in the "OFF" state reaches the target surface which may result in gripped object sticking to the EPM. This can be prevented, e.g. by a thin layer on the underside of the EPM device.

Last but not least, the holding force of the EPM has been calculated. In simulation, the holding force has been evaluated to be 12.60 N, which is lower than the holding force of 14.97 N calculated using the theoretical assumptions. The observed difference is probably caused by the leakage flux, which has been omitted in the theoretical part.

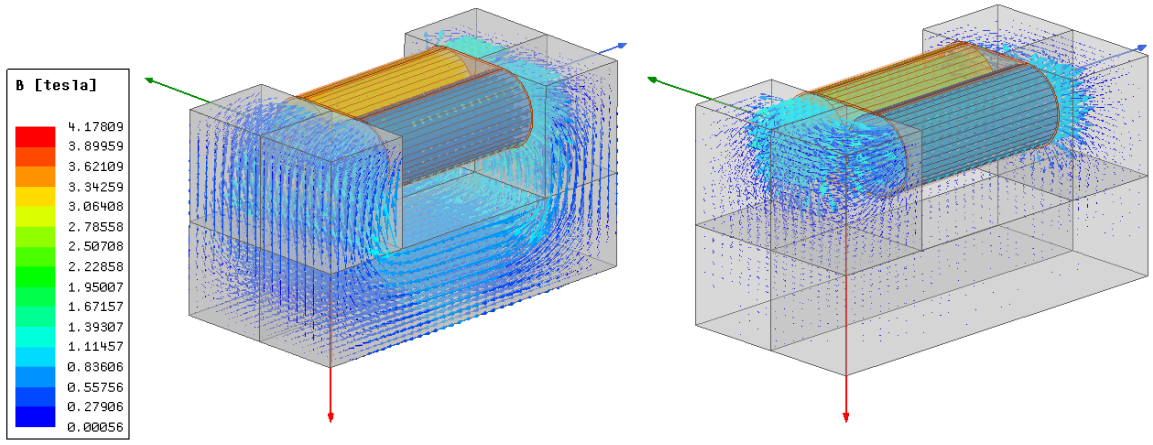

(a) The "ON" State. (b) The "OFF" State.

Figure 29: The EPM device model with the target surface. The direction of the magnetic flux density (and therefore the direction of the magnetic flux) is shown using a vector field. The size and the color of the arrows determine the value of the magnetic flux density.

4.2 Experimental Evaluation

A prototype of the EPM device has been manufactured to experimentally verify the derived results and to demonstrate the EPM device principle. Besides, it is important to get experience with the manufacturing process to discover potential pitfalls that can be expected when creating additional prototypes. Hence, a home-made prototype has been constructed according to the specifications listed in Table 3 that have been used for obtaining the simulation results as well.

4.2.1 Material of the Electropermanent Magnet Prototype

For the magnetic rods, the NdFeB and AlNiCo magnets were purchased from SELOS Magnetics, s.r.o. [33] with the properties of the magnets listed in [34] and [35]. The keeper bars have been made from an iron core of an old videorecorder head. The iron core has been cut into the keeper bars of the required size and the bars were abraded using sandpaper. Unfortunately, the precise magnetic properties of the iron core are unknown. The copper wire with the diameter of 0.5 mm has been used for the coil.

4.2.2 Manufacture Process

The dimensions of the EPM device for experimental evaluation cope with the properties listed in Section 3.5.1. First, it was necessary to join the magnets with the keeper bars. A two component epoxy adhesive has been used for creating the connection. The epoxy adhesion needed 24 hours for curing. The EPM device, after the curing of the epoxy adhesion, is shown in Figure 31a. Next, the magnet has been wounded with copper wire. The EPM device with the coil is shown in Figure 31b.

4.2.3 Experimental Setup

A control circuit has been developed for the evaluation of the EPM device to switch the EPM state by generation of a proper current pulse. The circuit uses a programmable micro-controller STM32F429I - DISCO [36], which generates a pulse of the proper length, that is connected to a circuit that drives the EPM according to the schematic shown in Figure 32. The micro-controller has been programmed to

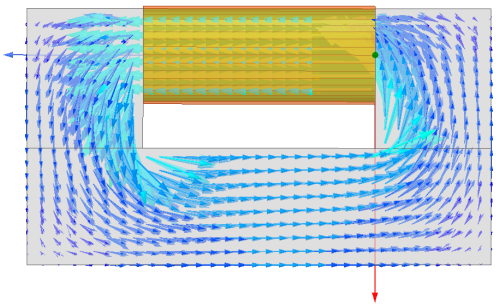

(a) The “ON” state - side view 1.

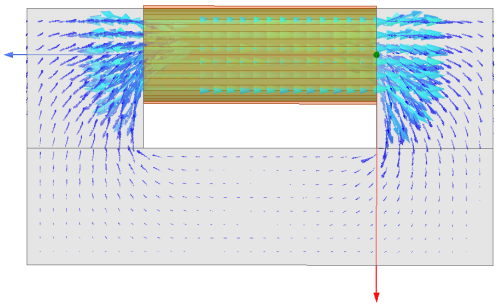

(b) The “OFF” state - side view 1.

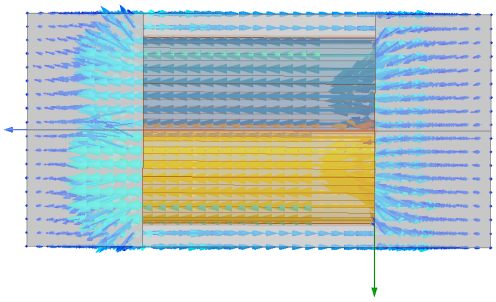

(c) The “ON” state - view from above.

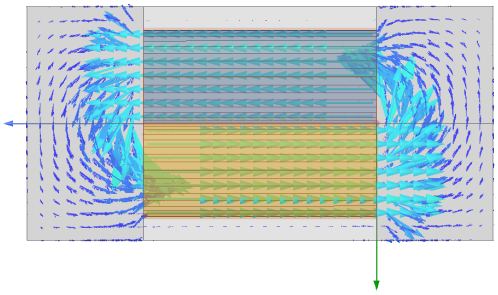

(d) The “OFF” state - view from above.

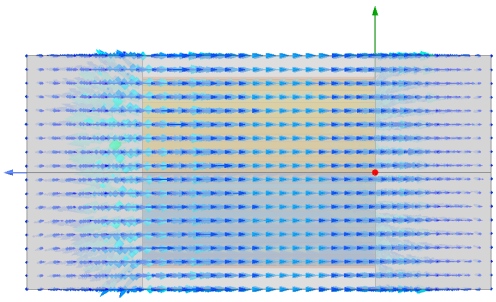

(e) The “ON” state - view from below.

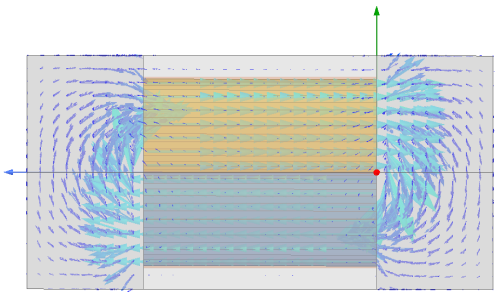

(f) The “OFF” state - view from below.

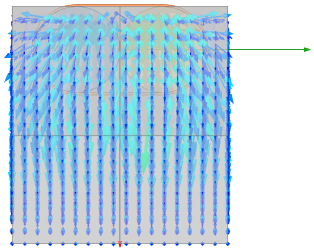

(g) The “ON” state - side view 2.

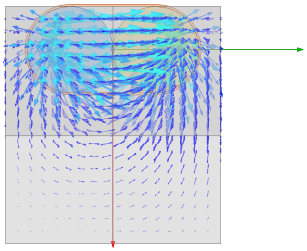

(h) The “OFF” state - side view 2.

Figure 30: The views of the EPM device model with the target surface. The direction of the magnetic flux density (and therefore the direction of the magnetic flux) is shown using a vector field. The size and the color of the arrows determine the magnitude of the magnetic flux density. The color scale is the same like in Figure 29.

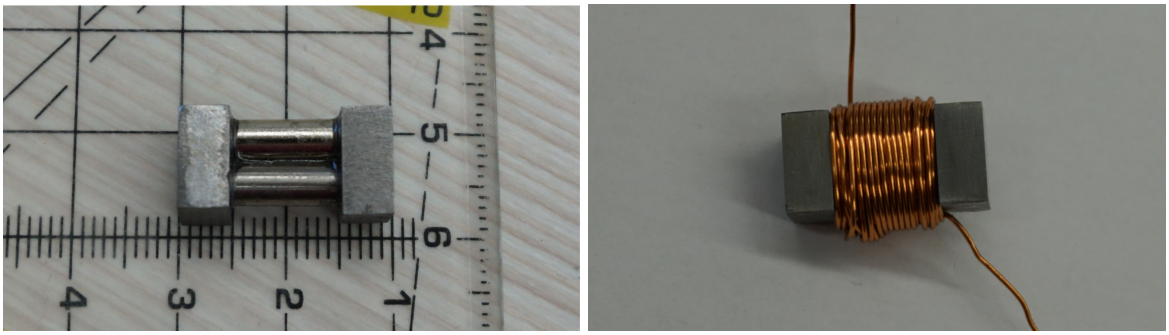

(a) The EPM device after curing of the epoxy adhesion. (b) The EPM device with the coil.

Figure 31: Process of the EPM device manufacturing.

send an impulse of a defined length over its GPIO pin when the user push-button is pressed. The length of the pulse to alternate the AlNiCo magnet orientation has been set according to Section 3.5.1 to be 320 μs which has been verified using the oscilloscope, as it is shown in Figure 33b. The generated pulse allows the current to flow from the battery with V_{DD} = 12 V through the R_3 = 2 Ω resistance to the EPM coil made from two 1 Ω resitors. The experimental setup is visualized in Figure 33a.

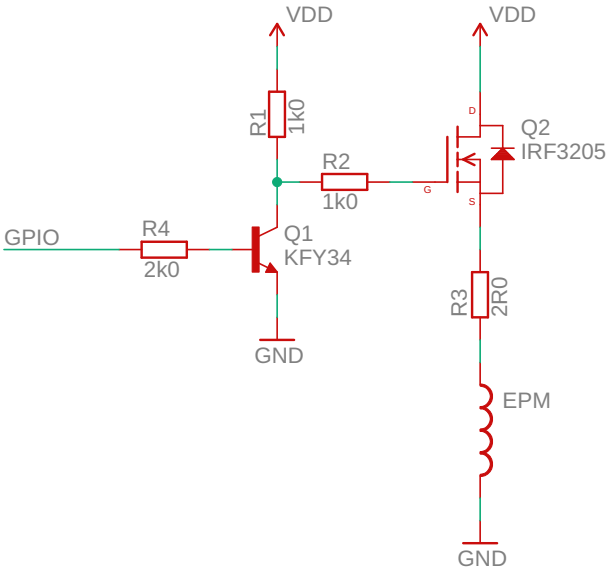

Figure 32: The schema of the control circuit.

4.2.4 Experiment Description and Results

The control circuit was connected with the EPM device and the trigger button was pressed. The holding force was tested, but the EPM device did not exhibit any change. Hence, the current pulse was measured and it was found that the current which flows through the coil is much lower than the required value. The required value of the current is 4.8 A, but the real value was 3.2 A, most likely due to the imprecise resistance of the 1 Ω resistors, which has been measured to be around 1.2 Ω each. Therefore, the control circuit was changed and the R_3 resistance has been altered to 1 Ω After that, the current value reached the 8.1 A with the same pulse length. The holding force of the EPM device was tested again. First, the EPM device was fully demagnetized, it means that the EPM device reached the "OFF" state. After that, the polarity of the current was changed and the EPM device was repolarizated

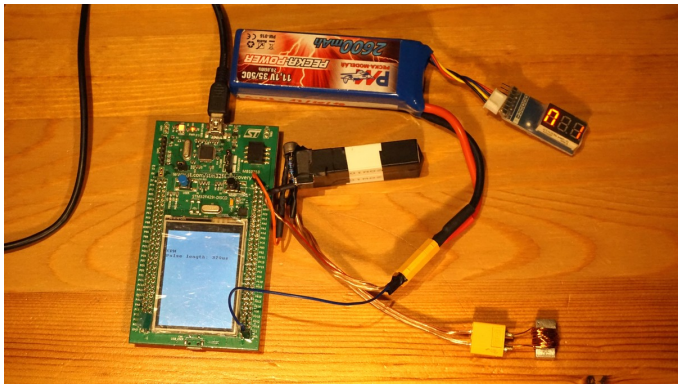

(a) The Experimental setup.

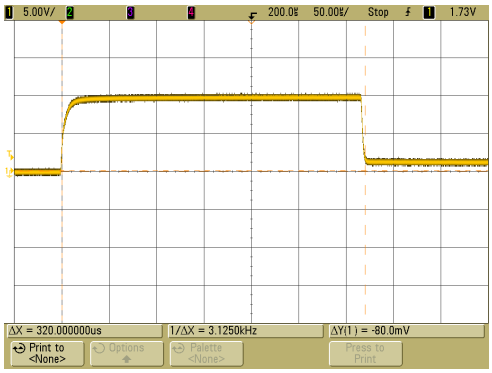

(b) The verification of the length of the switching pulse by oscilloscope.

Figure 33: The experimental setup for the evaluation of the 6EPM device.

to the "ON" state. The holding force was tested again and its value reached 1.28 N which is way below the theoretical results which is most likely because of the EPM manufacture precision. Hence, the resistance R_3 has been altered again to use parallel combination of the resistors to produce the resulting resistance of approx. 0.5 Ω. The current was not precisely measured, but it is assumed to be around 16.3 A. Finally, the maximal holding force reached the value of 7.34 N. The holding force has been evaluated using the scale, as it is shown in Figure 34. A metal plate of 1.4 kg mass has been placed on the scale together with the attached EPM device. Then, the plate has been slowly manually lifted up using EPM device as the handle up to the point where the EPM device detached from the plate. The maximum observed holding force has been recorded. The experiment has been repeated three times and in all cases the value of the holding force has been similar. The detailed discussion of the results is presented in the following section.

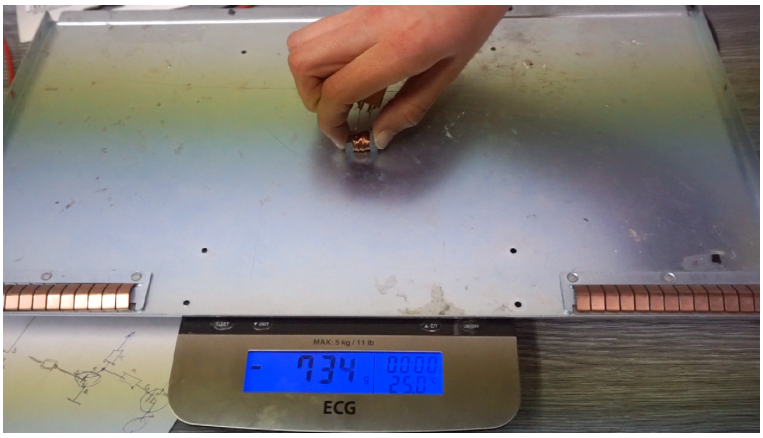

Figure 34: The scale with the highest value of the holding force.

4.3 Discussion

The values of expected holding force F_H from the theoretical assumptions, the simulations and from the experimental evaluation are summarized in Table 4.

First, it is necessary to realize a few things to explain the differences in the results. The theoretical calculation derives the maximal holding force given the simplifying assumptions, e.g. air gap is equal to zero, etc. Next, we neglect the leakage flux in the calculations, while the simulations take the leakage flux into account. Further, the simulation precision is influenced by a number of parameters

including, but not limited to, the number of iterations, the size of the mesh elements, the precise used type of the material (especially on the specific "B-H" curve of the material), etc. Nevertheless, similar results are obtained using the model and the simulation, but the experimental verification.

The result of the experimental evaluation is detrimental in comparison to the theoretical results. However, it is necessary to mention that the tested EPM device has been home-made. It means, that lot of problems had to be solved and a lot of unknown variables arose. The material properties for the keeper bars are unknown, and the holding surface has been machined by hand. Hence, the contact surfaces of the keeper bars are not perfectly flat which affect the quality of joining of the EPM device with the target surface. Further, the coil winding and epoxy curing may further influence the parameters of the prototype device. Nevertheless, the experimental verification proves the operational principle of the EPM device and brought insights into the process of the EPM manufacture.

Despite all the problems, an interesting thing has been observed. People who work with the electropermanent magnetic gripper [18] in practice reported that the light objects tend to stick to the keeper bars, most likely due to the leakage flux which flows through the EPM device even in the "OFF" state. Opposedly, we did not notice this phenomenon when experimenting with the developed EPM device.

Table 4: Holding force of the EPM device

	Value of the holding force F_{H} (N)
Theoretical assumptions	14.97
Simulation	12.60
Experiment 1	6.89
Experiment 2	7.34
Experiment 3	7.24

Chapter 5
Conclusion

The main goals of the thesis were to describe the principle of the electropermanent magnet, describe its use in practice and to evaluate the principle of the EPM by appropriate simulation model.

The first part of the thesis is focused on the principle of the electropermanent magnet, which is based on the combination of the permanent magnet and electromagnet by switching between a specific states of the EPM. The use of the EPM in practice was described as well as the applications of the EPM that are under the development. In addition, the advantages and disadvantages of the EPM and comparison to other technologies were listed.

The second part of this thesis described the operation of the EPM device and which material it is appropriate to use for design of the EPM device. The majority of this part focused on the design of the EPM device. The important parameters of the EPM device were derived and described so that a real EPM device can be designed on their basis. Further, the mathematical-physical relations described in Section 3.4 have been implemented in the programming language Python to visualize the dependencies of the aforementioned parameters and to help with finding the parametrization of the real EPM device. As the result of this implementation, it is possible to consider the theoretical value of the holding force of the designed real EPM device. This holding force was appointed to 14.97 N.

The third part of the thesis was motivated by evaluation of the theoretical knowledge with the realistic simulations. The simulations verified the switching between the “ON” and “OFF” states and the holding force from the simulation reached 12.6 N.

In addition to the set objectives of the thesis, the experimental verification was made. The EPM device prototype was created, as it is described in Section 4.2. The results of the experiment are that the prototype of the EPM device behaved as it was expected. Minor problems appeared during the evaluation of the holding force, which is thoroughly described in the discussion of the experiment results, but were solved. The maximal measured holding force of the constructed EPM device reached 7.34 N. Therefore, we are convinced that all the goals of the thesis were reached.

There is still a plenty of space for improvement of the EPM device design; however the thesis proved the validity of the concept and it may be the source for the future work on this topic. Regarding the future work, it is necessary to push the development of the EPM device prototype to find better materials for the construction. Next, it will be challenging to try to use the EPM device for novel actuators or artificial muscle tendons.

References

[1] J. Coey, "Magnetism in future," *Journal of Magnetism and Magnetic Materials*, vol. 226, pp. 2107–2112, 2001.

[2] "Elektronická učebnice @ONLINE," https://eluc.kr-olomoucky.cz/verejne/lekce/452, cited on 12/11/2018.

[3] "Encyklopedia Britannica, Inc. @ONLINE," https://www.britannica.com/science/Curie-point, cited on 12/11/2018.

[4] "InfoSpace Holdings LLC @ONLINE," https://science.howstuffworks.com/electromagnet.htm, cited on 12/11/2018.

[5] "VŠB - Technická universita Ostrava, Ložiska nerostů @ONLINE," http://geologie.vsb.cz/loziska/loziska/rudy/magnetit.html, cited on 12/11/2018.

[6] "PlatinMarket @ONLINE," http://www.dunyamagnet.com/buyuk-bar-miknatis-pmu168, cited on 12/11/2018.

[7] "Great Basin National Park Foundation @ONLINE," http://www.greatbasinobservatory.org/lesson-plans/build-electromagnet, cited on 12/11/2018.

[8] Z. Horák, F. Krupka, and V. Šindelář, *Technická fysika*. Státní nakladatelství technické literatury, 1961.

[9] "Elektronická učebnice @ONLINE," https://eluc.kr-olomoucky.cz/verejne/lekce/459, cited on 9/11/2018.

[10] "ElectronicsTutorial @ONLINE," https://www.electronics-tutorials.ws/electromagnetism/magnetic-hysteresis.html, cited on 28/10/2018.

[11] R. W. Messler, *Joining of materials and structures: from pragmatic process to enabling technology*. Butterworth-Heinemann, 2004.

[12] "Adams Magnetic Products Co. @ONLINE," https://www.adamsmagnetic.com/permanent-magnets-vs-electromagnets, cited on 25/11/2018.

[13] "Armstrong Magnetics, Inc. @ONLINE," https://www.armsmag.com/info-technical-data-lifting-magnets-knowledge-working-principles-eplm.html, cited on 25/11/2018.

[14] A. N. Knaian, "Electropermanent magnetic connectors and actuators: devices and their application in programmable matter," Ph.D. dissertation, Massachusetts Institute of Technology, 2010.

[15] "The Welding Institute @ONLINE," https://www.twi-global.com/technical-knowledge/faqs/faq-what-are-the-advantages-and-disadvantages-of-utilising-a-permanent-magnet-for-magnetic-particle-inspections/, cited on 25/11/2018.

[16] "Uptech engineering @ONLINE," http://www.magneticliftersindia.com/electro-permanent-magnetic-tilting-lifter-for-sheets.html, cited on 24/11/2018.

[17] G. Loianno, V. Spurny, J. Thomas, T. Baca, D. Thakur, D. Hert, R. Penicka, T. Krajnik, A. Zhou, A. Cho *et al.*, "Localization, grasping, and transportation of magnetic objects by a team of mavs in challenging desert like environments," *IEEE Robotics and Automation Letters*, vol. 3, no. 3, pp. 1576–1583, 2018.

[18] "Multi-robots System, CTU in Prague @ONLINE," http://mrs.felk.cvut.cz/mbzirc, cited on 26/11/2018.

[19] P. Ward and D. Liu, "Design of a high capacity electro permanent magnetic adhesion for climbing robots," in *IEEE International Conference on Robotics and Biomimetics (ROBIO)*, 2012, pp. 217–222.

[20] T. Bandyopadhyay, R. Steindl, F. Talbot, N. Kottege, R. Dungavell, B. Wood, J. Barker, K. Hoehn, and A. Elfes, "Magneto: A versatile multi-limbed inspection robot," in *IEEE/RSJ International Conference on Intelligent Robots and Systems (IROS)*, 2018, pp. 2253–2260.

[21] W. Shen, J. Gu, and Y. Shen, "Permanent magnetic system design for the wall-climbing robot," *Applied Bionics and Biomechanics*, vol. 3, no. 3, pp. 151–159, 2006.

[22] H. Kurokawa, A. Kamimura, E. Yoshida, K. Tomita, S. Murata, and S. Kokaji, "Self-reconfigurable modular robot (m-tran) and its motion design," in *International Conference on Control, Automation, Robotics and Vision (ICARCV)*, vol. 1, 2002, pp. 51–56.

[23] A. N. Knaian, K. C. Cheung, M. B. Lobovsky, A. J. Oines, P. Schmidt-Neilsen, and N. A. Gershenfeld, "The milli-motein: A self-folding chain of programmable matter with a one centimeter module pitch," in *IEEE/RSJ International Conference on Intelligent Robots and Systems (IROS)*, 2012, pp. 1447–1453.

[24] J. Tugwell, P. Brennan, C. O'Shea, K. O'Donoghue, T. Power, M. O'Shea, J. Griffiths, R. Cahill, and P. Cantillon-Murphy, "Electropermanent magnetic anchoring for surgery and endoscopy," *IEEE Transactions on Biomedical Engineering*, vol. 62, no. 3, pp. 842–848, 2015.

[25] J. P. Rigla *et al.*, "Multi-coil shimming system for an electropermanent magnet mri system," in *ESMRMB Annual Scientific Meeting*. European Society for Magnetic Resonance in Medicine and Biology, 2017.

[26] Z. Zhakypov and J. Paik, "Design methodology for constructing multimaterial origami robots and machines," *IEEE Transactions on Robotics*, vol. 34, no. 1, pp. 151–165, 2018.

[27] S. Miyashita, S. Guitron, M. Ludersdorfer, C. R. Sung, and D. Rus, "An untethered miniature origami robot that self-folds, walks, swims, and degrades," in *IEEE International Conference on Robotics and Automation (ICRA)*, 2015, pp. 1490–1496.

[28] A. E. Fitzgerald, C. Kingsley, S. D. Umans, and B. James, *Electric machinery*. McGraw-Hill New York, 2003, vol. 5.

[29] V. Pankrác, "Pomocné texty k přednáškám z teorie elektromagnetického pole," ZS 2015/2016.

[30] "ANSYS, Inc. @ONLINE," https://www.ansys.com/products/all-products, cited on 17/12/2018.

[31] "Wikimedia Foundation, Inc. @ONLINE," https://en.wikipedia.org/wiki/Finite_element_method, cited on 17/12/2018.

[32] "Lecture of the Numerical Analysis of Structures, CTU in Prague, Faculty of the civil enegineering @ONLINE," https://mech.fsv.cvut.cz/homeworks/student/NAK/lecture01.pdf, cited on 17/12/2018.

[33] “SELOS Magnetics, s.r.o. @ONLINE,” https://www.magnety.cz/magneticke-materialy/, cited on 31/12/2018.

[34] “SELOS Magnetics, s.r.o. @ONLINE,” https://www.magnety.cz/neodymy/neodym-disk-anizotrop/, cited on 31/12/2018.

[35] “SELOS Magnetics, s.r.o. @ONLINE,” https://www.magnety.cz/magneticke-materialy/alnico-500-tyc-anizotrop/, cited on 31/12/2018.

[36] “Arm Limited @ONLINE,” https://os.mbed.com/platforms/ST-Discovery-F429ZI/#board-pinout, cited on 1/1/2018.